MESSENGER Observations of Standing Whistler Waves Upstream of Bow Shock of Mercury

Yang Wang[1], Jun Zhong[2], James A. Slavin[3], Hui Zhang[2], Lou-Chuang Lee[4], Lican Shan[2], Yong Wei[2], and Yongxin Pan[2]

[1]Key Laboratory of Earth and Planetary Physics, Institute of Geology and Geophysics, Chinese Academy of Sciences
[2]Institute of Geology and Geophysics, Chinese Academy of Sciences
[3]University of Michigan-Ann Arbor
[4]Institute of Earth Sciences

December 17, 2022

Abstract

This paper reports on the standing whistler waves upstream of Mercury's quasi-perpendicular bow shock. Using MESSENGER's magnetometer data, 36 wave events were identified during interplanetary coronal mass ejections (ICMEs). These elliptic or circular polarized waves were characterized by: (1) a constant phase with respect to the shock, (2) propagation along the normal direction to the shock surface, and (3) rapid damping over a few wave periods. We inferred the speed of Mercury's bow shock as ˜31 km/s and a shock width of 1.76 ion inertial length. These events were observed in 20% of the MESSENGER orbits during ICMEs. We conclude that standing whistler wave generations at Mercury are generic to ICME impacts and the low Alfvén Mach number (MA) collisionless shock, and are not affected by the absolute dimensions of its bow shock. Our results further support the theory that these waves are generated by the current in the shock.

Hosted file

952282_0_art_file_10542172_rmz7xj.docx available at https://authorea.com/users/567100/articles/613608-messenger-observations-of-standing-whistler-waves-upstream-of-bow-shock-of-mercury

MESSENGER Observations of Standing Whistler Waves Upstream of Bow Shock of Mercury

Yang Wang[1,2], Jun Zhong[1,2], James Slavin[3], Hui Zhang [1,2], Lou-Chuang Lee[4,5], Lican Shan[1,2], Yong Wei[1,2], Yongxin Pan[1,2]

[1]Key Laboratory of Earth and Planetary Physics, Institute of Geology and Geophysics, Chinese Academy of Sciences, Beijing, China

[2]College of Earth and Planetary Sciences, University of Chinese Academy of Sciences, Beijing, China

[3]Department of Climate and Space Sciences and Engineering, University of Michigan, Ann Arbor, Michigan, USA

[4]Institute of Earth Sciences, Academia Sinica, Taipei, Taiwan

[5]State Key Laboratory of Lunar and Planetary Sciences, Macau University of Science and Technology, Macau, China

Correspondence to: Jun Zhong (j.zhong@mail.iggcas.ac.cn)

Key Points:

- We identify 36 Mercury's bow shock crossings with standing whistler waves during interplanetary coronal mass ejection intervals.
- The amplitude, polarization, and damping length of the standing whistler waves were identified and statistically analyzed.
- These standing whistler waves may be generated by currents in shock, and the shock is not the largest-amplitude circle of the waves.

Abstract

This paper reports on the standing whistler waves upstream of Mercury's quasi-perpendicular bow shock. Using MESSENGER's magnetometer data, 36 wave events were identified during interplanetary coronal mass ejections (ICMEs). These elliptic or circular polarized waves were characterized by: (1) a constant phase with respect to the shock, (2) propagation along the normal direction to the shock surface, and (3) rapid damping over a few wave periods. We inferred the speed of Mercury's bow shock as ~31 km/s and a shock width of 1.76 ion inertial length. These events were observed in 20% of the MESSENGER orbits during ICMEs. We conclude that standing whistler wave generations at Mercury are generic to ICME impacts and the low Alfvén Mach number (M_A) collisionless shock, and are not affected by the absolute dimensions of its bow shock. Our results further support the theory that these waves are generated by the current in the shock.

Plain Language Summary

The strength of planetary bow shocks varies with the planet's heliocentric distance from the Sun. Studying the bow shocks of other planets is important for extending our understanding of collisionless-shock physics. In the solar system, the bow shocks of Mercury are unique as they are produced by low Mach numbers and low plasma beta solar wind blowing over a small magnetized body that is 1–2 orders smaller than Earth. The standing whistler waves upstream of the bow shock of Mercury were determined through statistical analyses. Similar to the observations at Earth, these waves were rapidly damping with a proportion of the wave periods; however, the damping distance at the spacecraft frame was considerably shorter at only a few kilometers upstream in the small-scale bow shock of Mercury. The high occurrence rate of standing whistler waves suggests that Mercury's bow shock is a natural plasma laboratory, which can be used to further investigate low M_A planetary shocks during the upcoming BepiColombo mission.

1 Introduction

Whistler waves are common upstream features of planetary bow shocks and are involved in shock formation and particle interactions (Balogh et al., 2013; Oka et al., 2017; Oka et al., 2019). Two types of whistler waves emitting from shock ramps have been previously identified: propagating and phase standing (Russell et al., 1995). The propagation direction of propagating whistler waves has a small angle with the magnetic field and they propagate far upstream (Russell et al., 2007). They have been widely observed upstream of the bow shock of Earth and are typically called “1 Hz” waves. Furthermore, they are also commonly observed in other planetary shocks, such as those of Mercury, Venus, Mars, and Saturn (Fairfield et al., 1976; Orlowski et al., 1991; Le et al., 2013; Sulaiman et al., 2017; Ruhunusiri et al., 2018). In contrast, phase standing whistler waves are generated when the wave propagation speed equals the component of the solar wind velocity that is normal to the bow shock (Perez et al., 1970). They propagate along the shock-normal direction at a constant phase with respect to the shock ramp and can rapidly damp within a few wave periods. The right-handed wave polarization relative to its average field direction is a key observational feature, when an observer moves upstream to downstream. In contrast, the left-handed wave polarization can be observed when the observer moves in the opposite direction. Standing whistler waves have been rarely observed upstream of the bow shock of the Earth (e.g., Fairfield et al., 1975; Mellott et al., 1984; Farris et al., 1993) as they commonly occur under low M_A conditions, such as during an ICME passage.

Mercury has a miniature and weak bow shock, which is created by the interaction of low Mach number solar wind and a relatively small planetary magnetosphere in the inner hemisphere. The average bow shock subsolar distance has been determined to be only ~2 R_M (radius of Mercury, 1 R_M = 2440 km), which is approximately 1–2 orders smaller than that of the Earth (Winslow et al., 2013). The “1 Hz” whistler waves have been commonly observed upstream of the bow shock of Mercury (Fairfield et al., 1976; Le et al., 2013), in which they propagate along the magnetic field and farther upstream (~30000 km). Although phase standing whistler waves have been observed at Mercury, they have not yet been analyzed (Gedalin et al., 2022).

Due to the nature of close-in orbit, there is higher probability for observing low M_A shocks at Mercury than other planets. The typical M_A at Mercury orbit is ~4-6 (Slavin et al., 1981). Especially, the M_A can be less than 3 during ICMEs (Liu et al., 2005; Sarantos et al., 2009). The ICME impact on Mercury’s magnetosphere was first analyzed by Slavin et al. (2014). They showed that Mercury’s dayside magnetosphere is highly dynamic and greatly compressed by ICME impacts. The bow shock and magnetopause reconfigurations during the impact of ICMEs deviates greatly from normal conditions (Slavin et al., 2014; Winslow et al., 2015; 2017), and the dayside magnetosphere may even occasionally disappeared (Slavin et al., 2019;

Winslow et al., 2020). MESSENGER orbited Mercury during the maximum of solar cycle 24. Over the four-year mission from February 2011 to April 2015, a total of 69 ICMEs were detected by MESSENGER (Winslow et al. 2015, 2017). We use the 69 ICMEs to study standing whistler waves.

Here we report the MESSENGER observations of the standing whistler wave upstream Mercury's bow shock during ICMEs collated by Winslow et al. (2015, 2017). Among 69 ICMEs, we identified 36 standing whistler wave events corresponding to at least 20% of the orbits. Our results suggest that Mercury is a natural plasma laboratory for the understand the physics of standing whistler waves and low M_A collisionless shocks. It is likely that our understanding of such low Mach number shocks will be greatly advanced by measurements to be collected by the upcoming Bepi-Colombo mission.

2 Case Analysis of Standing Whistler Wave

The dynamics of dayside magnetosphere and magnetotail response to an ICME observed by MESSENGER on November 23, 2011 have been analyzed in detail by Slavin et al. (2014) and Zhong et al. (2020), respectively. This study analyzes its effects on the bow shock. Figures 1a–d show an overview of MESSENGER's bow shock crossings during this ICME. High-resolution magnetic field data (20 vectors s^{-1}) obtained from the magnetometer (MAG; Anderson et al., 2007) were used and displayed in the aberrated Mercury solar magnetic (MSM) coordinates. The MSM coordinate system was centered on the offset internal dipole of Mercury (Anderson et al., 2011), wherein the X-axis was pointed toward the Sun, the Y-axis was pointed in the opposite direction of the orbit motion, and the Z-axis completed the right-handed system. The average radial solar wind speed of 700 km s^{-1} during the ICME was applied to correct for the aberration. The spacecraft crossed the bow shock thrice; the crossings are denoted as inbound crossing 1, outbound crossing, and inbound crossing 2 in Figure 1. The multiple crossings may be attributed to the temporal variations of the upstream solar wind conditions.

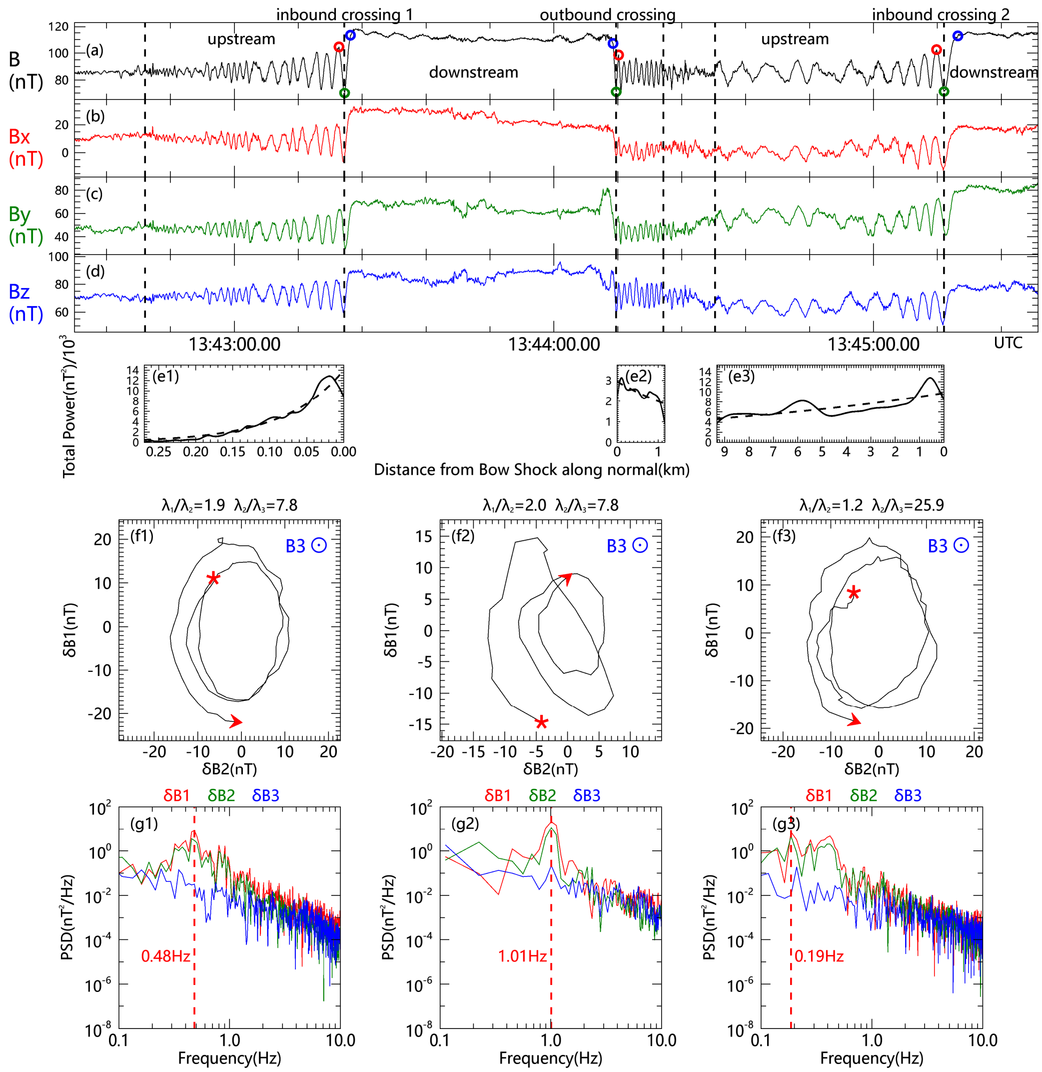

Figure 1. MESSENGER observations of standing whistler waves upstream of the bow shock of Mercury during the ICME on 23 November 2011. **(a)–(d)** Magnetic field strength and its three components in the aberrated MSM coordinate system; the red, green, and blue dots correspond to the peak, wave trough, and end of the shock ramp, respectively. **(e)** Total power as a function of the distance from the bow shock along shock normal. **(f)–(g)** Magnetic field data of the wave in the maximum-intermediate plane and the power spectral density in the minimum variance analysis (MVA) after removing the background magnetic field. The T_{ramp} refers to the interval time between the blue and green dots. The T_{wave} refers to twice the interval time between the red and green dots.

The shock normal was determined using the magnetic coplanarity method (Lepping et al., 1971) that substitutes the average magnetic field upstream and downstream of the shock; it is expressed as $\boldsymbol{n} = \frac{(\boldsymbol{B_1} \times \boldsymbol{B_2}) \times (\boldsymbol{B_2} - \boldsymbol{B_1})}{|(\boldsymbol{B_1} \times \boldsymbol{B_2}) \times (\boldsymbol{B_2} - \boldsymbol{B_1})|}$. The shock normals for the inbound crossing 1, outbound crossing, and inbound crossing 2 were observed to be very close at (0.56, -0.05, -0.82), (0.71, -

0.02, -0.70), and (0.76, -0.06, -0.65), respectively, and their mean upstream magnetic fields were (9.24, 46.57, 72.37), (2.40, 45.41, 71.94), and (1.33, 55.94, 64.86) nT, respectively. The angles between the mean upstream magnetic field $\mathbf{B_{up}}$ and the shock normal **n** were θ_{Bn} = 49.13°, 52.23°, and 58.49°, indicating quasi-perpendicular shocks.

The accompanying upstream waves are considered key features of these bow shock crossings. The polarizations and vectors of these waves were obtained from the results of the minimum variance analysis (MVA) of the magnetic field within an upstream wave time interval (Sonnerup et al., 1967). Using these, the direction of propagation for an assumed planar wave can be estimated. For inbound crossing 1, the small ratio of the maximum to intermediate eigenvalues λ_1/λ_2 = 1.9 and the large ratio of the intermediate to minimum eigenvalues λ_2/λ_3 = 7.8 suggest that the waves had relatively stable elliptic polarizations. The wave vector **k** corresponds to the minimum variance eigenvector $\mathbf{e_3}$ (0.70, -0.11, -0.69), whereas the corresponding mean magnetic field ($\mathbf{B_0}$) is directed out of the maximum-intermediate plane. The hodograms of the magnetic field for several wavelengths in the MVA coordinates are shown in Figure 1f. The gyration of the magnetic field with respect to $\mathbf{B_0}$ indicates that the wave polarization was right-handed in the spacecraft coordinate frame (SCF). The angles between **k** and **n** (θ_{kn}) and **k** and $\mathbf{B_{up}}$ (θ_{kB}) were 11.85° and 55.49°, respectively, wherein the small θ_{kn} and large θ_{kB} suggest that the wave propagated approximately along the shock normal direction rather than the magnetic field.

The waves observed during the outbound crossing and inbound crossing 2 were also elliptically polarized (Figures 1f2 and f3), with θ_{kn} = 23.18°, 2.82° and θ_{kB} = 64.17°, 58.14°, respectively. Moreover, the polarization direction of the outbound crossing was opposite to that of the inbound crossing, wherein it was left-handed, which is consistent with the characteristics of standing whistler waves (Fairfield et al., 1975; Mellott et al., 1984).

Wavelet analysis was used to calculate the total power at each moment. Figure 1e shows the variations of the total power along **n** in the SCF. The function $P = P_0e^{-T/T0}$ was fit to the total power. For inbound crossing 1, the damping time (T_0) was 11.17 s, which was 5.32 times the wave period (T_{wave}), indicating rapid damping. The damping distance was 1.83 km along **k** and the normalized wave amplitude ($\delta B_{wave}/B_u$) was 0.40. This rapid damping of waves was also observed during the outbound crossing and inbound crossing 2.

The power spectral density shown in Figure 1e demonstrates that these waves were mainly restricted to the plane perpendicular to $\mathbf{e_3}$, as indicated by the PSD_1, and $PSD_2 \gg PSD_3$ around the wave frequency (f_{sc}) in the SCF. The f_{sc} for the inbound crossing 1, outbound crossing, and inbound crossing 2 were ~0.48, 1.01, and 0.19 Hz, respectively; the different values indicate the change in the relative velocity between the spacecraft and bow shock in the normal direction.

3 Statistical Results and Discussion

3.1 Statistical Results

We use 69 ICMEs (94 orbits) collated by Winslow et al. (2015, 2017) to find bow shock crossings during ICMEs. As standing whistler waves typically occur upstream of the quasi-perpendicular bow shock, the θ_{Bn} was calculated, wherein 486 quasi-perpendicular bow shock crossings ($\theta_{Bn} > 45°$) were identified to select the events. Multiple bow shock crossings are common during inbound or outbound crossings in each orbit owing to the up-and-down displacement of the shocks. MVA was performed on the magnetic field data upstream for each quasi-perpendicular shock crossing under the assumption that the eigenvalues conform to $\lambda_1/\lambda_2 < 2$ and $\lambda_2/\lambda_3 > 7$, which indicate that the waves are elliptically or circularly polarized. In all elliptically polarized waves, 36 perpendicular bow shock crossings with rapid damping were identified, including 20 inbound and 16 outbound crossings. They occurred during 19 orbits, with an orbital occurrence rate of ~20%.

The characteristics of the wave during each event were observed (Supplement Table 1). A statistical analysis indicated the following:

Wave polarization. Right-handed polarization was observed in 16 of the 20 upstream to downstream traversals, whereas left-handed polarization was observed in all 16 downstream to upstream traversals. These polarizations were consistent with the previous theory and observation of standing whistler waves presented by Perez et al. (1970) and Fairfield et al. (1975).

Propagation direction. The calculated θ_{kn} ranged from ~0° to 50°, while the θ_{kB} ranged from ~45° to 90° (Figure 2a). The mean θ_{kn} and θ_{kB} were 17.31° and 69.55°, respectively. These results suggest that the waves were propagating along the shock normal instead of the magnetic field. These results are also consistent with the observations at Earth (Mellott et al., 1984); however, they are different from the propagating direction of “1 Hz” waves observed at Mercury (Fairfield et al., 1976; Le et al., 2013).

Wave damping. Figure 2b shows the distance from the wave damping to e^{-1} to the ramp on the **n** in the SCF, wherein the amplitudes of most waves damp at e^{-1} within 10 km. This was significantly less than the damping distance of the “1 Hz” wave within ~30000 km at Mercury (Le et al., 2013). The ratio of T_0 and T_{wave} was nearly <10 (Figure 2c). The standing whistler waves on Earth also exhibit this rapid damping, which is <10 times the wave periods (Mellott et al., 1984); hence, the damping mechanism can be considered as Landau damping (Gary et al., 1985).

Wave frequency. The mean frequency of standing whistler waves was 1.67 Hz in the SCF. Here, 70% of the events had a frequency <2 Hz (Figure 2d), suggesting that the standing whistler waves have a lower frequency than the “1 Hz” waves at Mercury (2–3 Hz, Russell, 2007).

Based on the statistical results of these events, it was discovered that its characteristics were similar with those of the standing whistler wave. Meanwhile, other properties (Figures 2e and f) of the waves are described in detail in the Discussion Section.

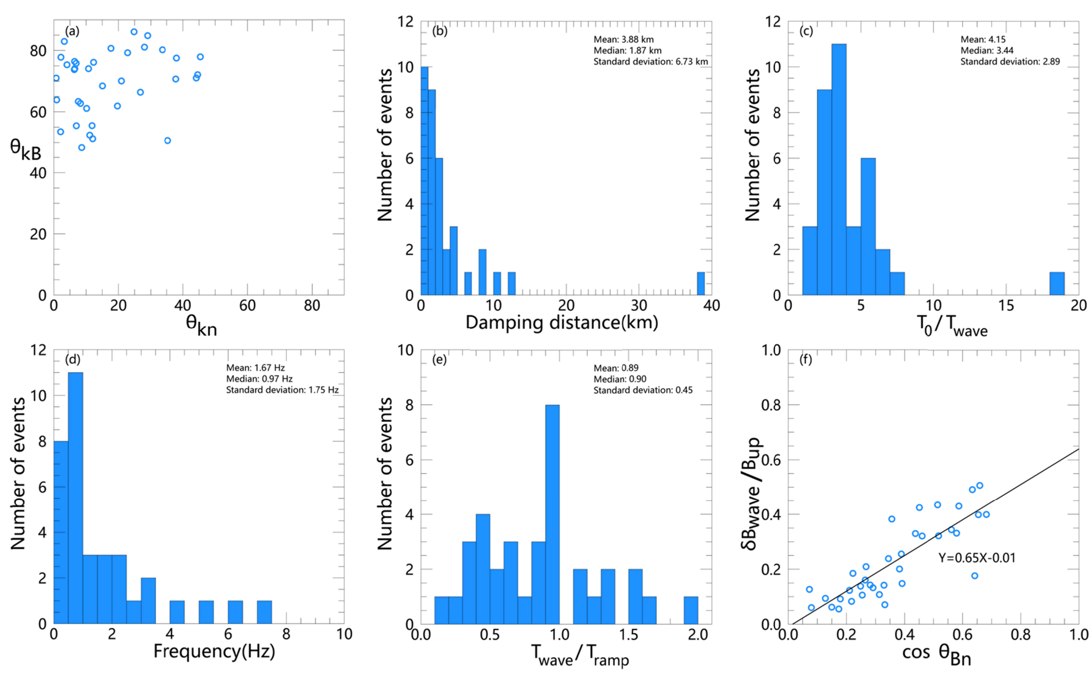

Figure 2. Statistical properties of the standing whistler waves upstream of the bow shock of Mercury. **(a)** Occurrence of events as functions of θ_{kn} and θ_{kB}. **(b)–(e)** Distributions of damping distance, T_0/T_{wave}, frequency, and T_{wave}/T_{ramp}. **(f)** Correlation between θ_{Bn} and $\delta B_{wave}/B_{up}$.

Considering that the solar wind beam view of MESSENGER's fast imaging plasma spectrometer was obstructed by the sunshade, the upstream solar wind M_A could not deviate directly. The M_A was approximatively estimated using the following formula: $M_A - 1 = (B_{down}/B_{up} - 1)\ \sin^2\theta_{Bn}$, which is suitable for low Mach number and low-β shocks. (Balikhin et al., 2008). The magnetic field compression ratio (B_{down}/B_{up}: magnetic field intensity (average value of ~1 min) ratio of downstream to upstream) of all perpendicular bow shock crossings during ICMEs are plotted in Figure 3a, wherein it can be observed that most of the identified wave events (blue) had lower magnetic field compression ratios than the mean ratio during ICMEs. The distributions of the calculated M_A and wave event occurrence rates are plotted in Figure 3b, wherein the occurrence rate can be observed to increase as M_A decreases; 89% of the wave events obtained lower M_A values than the average value during ICMEs. Therefore, these waves have a high likelihood of occurrence under a relatively lower Mach number.

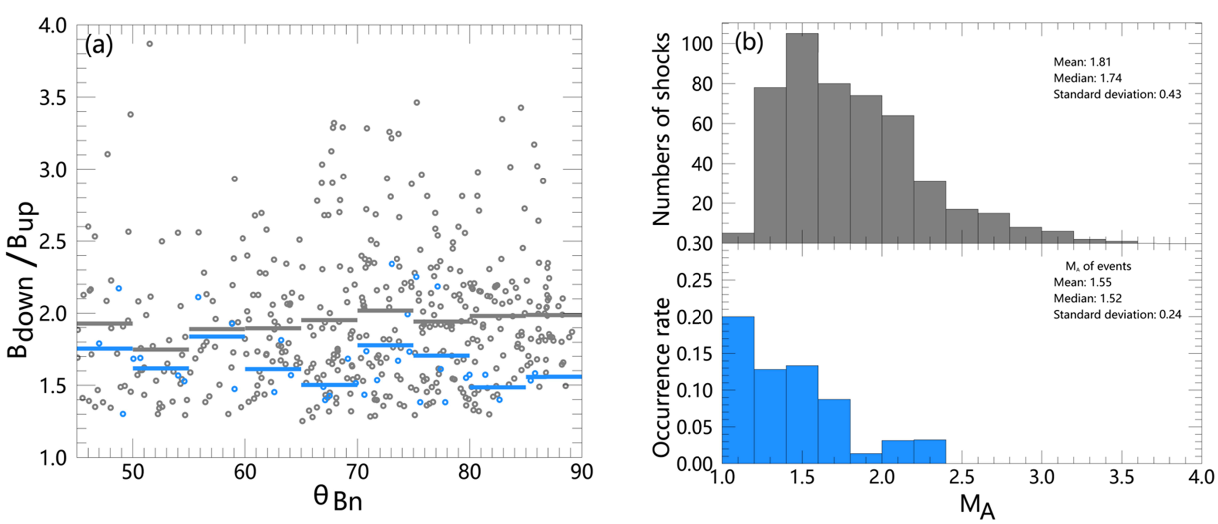

Figure 3. **(a)** Variations of the magnetic field compression ratio with θ_{Bn}. The gray and blue lines represent the average values of all shocks and wave events, respectively. **(b)** Distributions of M_A (top) and events occurrence rates (bottom; Unit : Number of events/Number of shocks in each M_A bin).

3.2 Discussion

On Earth, the theoretical wavelengths of standing whistler waves are consistent with those observed by Mellott et al. (1984). Hence, single spacecraft observations are normally used to infer the bow shock speed (Fairfield et al., 1975) based on theoretical predictions of the wavelength (Tidman et al., 1971): $\lambda = \frac{2\pi c \cos\theta_{Bn}}{\omega_{pi}({M_A}^2 - 1)^{1/2}}$, where ω_{pi} is the proton plasma frequency. By applying the typical values from the ICME model at 0.38 AU (Liu et al., 2005), $\omega_{pi} = 10034\, rad/s$, mean $M_A = 1.55$, and mean $\theta_{Bn} = 68°$ of all wave events, the theoretically predicted wavelength of $\lambda = \sim 59$ km was calculated. The average T_{wave} was ~1.89 s; hence, the shock speed (λ/T_{wave}) can be inferred as ~31 km/s. Notably, this was slightly less than the shock speed of ~40 km/s estimated through overshoot observations under normal conditions (Masters et al., 2015).

The shock ramp scale was also estimated using the scale relationship between the standing whistler waves and the shock ramps. A shock ramp scale of 53 km was obtained using the formula $\lambda \times T_{ramp}/T_{wave}$ (59 km × 0.89). Considering an ion inertial length (c/ω_{pi}) of 30 km, the width of the ramp was 1.76 c/ω_{pi}. Based on the results of Hobara et al. (2010), the scale can be larger than 1 c/ω_{pi} when M_A is low.

Previous theories have suggested that standing whistler waves are generated by a stable current in the shock ramp, from which the formula for the wave amplitude can be derived (Tidman et al., 1971). This theory suggests that $\delta B_{wave}/B_{up}$ has a positive correlation with $\cos\theta_{BN}$, and this relationship is demonstrated in Figure 2f. The best linear fit produced Y = [0.65±0.15]X - [0.01±0.06], which was also consistent with this theory. Based on the fitted values, the maximum amplitude of the standing whistler wave was approximately 0.8 times the intensity of the background magnetic field.

The shock is hypothesized to be the largest-amplitude circle of the upstream standing whistler wave, wherein its width is half of the wavelength. However, this results in conflicting ratios of the standing whistler wave wavelength to the shock thickness at Earth and interplanetary shock, as some researchers have estimated this ratio to be two (Goncharov et al., 2014) while others have estimated it to be closer to one (Mellott et al., 1984; Farris et al., 1993). In the SCF, the ratio between the period (T_{wave}) of the upstream whistler waves and the shock ramp crossing time (T_{ramp}) can be a good approximation of the shock width to wavelength ratio. Figure 2e shows the T_{wave}/T_{ramp} in the spacecraft frame of the upstream standing whistler waves of Mercury. In cases where T_{wave} was less than $2\times T_{ramp}$, the average ratio of the two was 0.89, indicating that the initial hypothesis must be reexamined to further determine the scale of the relationship between standing whistler waves and shock ramps.

4 Conclusions

In this study, we reported and statistically analyzed the standing whistler waves upstream of the bow shock of Mercury during ICMEs. These waves occur at lower M_A and propagate along the normal of the bow shock. It was observed that, similar to the waves at Earth, these waves were rapidly damping with few wave periods; however, the damping distance in SCF was significantly shorter, only a few kilometers upstream of the bow shock of Mercury. Our results support that these waves are generated by the current in the shock and that the shock is not the largest-amplitude circle of the waves. Hence, the generation of standing whistler waves was determined to be generic to the low Mach number collisionless shock. Additionally, a high occurrence rate of the standing whistler waves observed during ICMEs suggests that the bow shock of Mercury can be a natural plasma laboratory that can be used to further study low M_A planetary shocks. Considering that BepiColombo will arrive at Mercury in 2025 during the ascending and maximum phases of solar cycle 25, it is expected to encounter a large number of ICMEs. This study provides an understanding of standing whistler wave generation and their underlying physics, which can be used for the upcoming high-resolution BepiColombo observations.

Acknowledgments

This work was supported by the National Natural Science Foundation of China (41621004), and the Key Research Program of the Institute of Geology & Geophysics, CAS (Grant No. IGGCAS-201904 and IGGCAS-202102). J. A. Slavin acknowledges support from NASA grants 80NSSC18K1137, 80NSSC21M0364 and 80NSSC21K0052. L. C. Lee was supported by the Science and Technology Development Fund (FDCT) of Macau (0035/2018/AFJ) and the Ministry of Science and Technology, Taiwan (MOST 110-2111-M-002-017). MESSENGER data are available from the Planetary Data System (MAG).

Open Research

The MESSENGER MAG data used in this study are available at NASA's Planetary Data System:

https://pds-ppi.igpp.ucla.edu/search/view/?f=yes&id=pds://PPI/mess-mag-calibrated/data/mso;

The list of the identified standing whistler wave events is available in the supplemental information for the purposes of peer review. The data will eventually be deposited at NSSDC Space Science Article Data Repository (https://sadr-en.nssdc.ac.cn) by the time it is accepted.

References

Anderson, B. J., Acuña, M. H., Lohr, D. A., Scheifele, J., Raval, A., Korth, H., & Slavin, J. A. (2007). The Magnetometer instrument on MESSENGER. In *The MESSENGER mission to Mercury* (pp. 417-450). Springer, New York, NY. https://doi.org/10.1007/s11214-007-9246-7

Anderson, B. J., Johnson, C. L., Korth, H., Purucker, M. E., Winslow, R. M., Slavin, J. A., ... & Zurbuchen, T. H. (2011). The global magnetic field of Mercury from MESSENGER orbital observations. *Science*, *333*(6051), 1859-1862. https://doi.org/10.1126/science.1211001

Balikhin, M. A., Zhang, T. L., Gedalin, M., Ganushkina, N. Y., & Pope, S. A. (2008). Venus Express observes a new type of shock with pure kinematic relaxation. *Geophysical Research Letters*, *35*(1). https://doi.org/10.1029/2007GL032495

Balogh, A., & Treumann, R. A. (2013). *Physics of collisionless shocks: space plasma shock waves*. Springer Science & Business Media.

Fairfield, D. H., & Feldman, W. C. (1975). Standing waves at low Mach number laminar bow shocks. *Journal of Geophysical Research*, *80*(4), 515-522. https://doi.org/10.1029/JA080i004p00515

Fairfield, D. H., & Behannon, K. W. (1976). Bow shock and magnetosheath waves at Mercury. *Journal of Geophysical Research*, *81*(22), 3897-3906. https://doi.org/10.1029/JA081i022p03897

Farris, M. H., Russell, C. T., & Thomsen, M. F. (1993). Magnetic structure of the low beta, quasi-perpendicular shock. *Journal of Geophysical Research: Space Physics*, *98*(A9), 15285-15294. https://doi.org/10.1029/93JA00958

Gary, S. P., & Mellott, M. M. (1985). Whistler damping at oblique propagation: Laminar shock precursors. *Journal of Geophysical Research: Space Physics*, *90*(A1), 99-104. https://doi.org/10.1029/JA090iA01p00099

Gedalin, M., Golbraikh, E., Russell, C. T., & Dimmock, A. P. (2022). Theory helps observations: determination of the shock mach number and scales from magnetic measurements. *Frontiers in Physics*, 149. https://doi.org/10.3389/fphy.2022.852720

Greenstadt, E. W., Russell, C. T., Scarf, F. L., Formisano, V., & Neugebauer, M. (1975). Structure of the quasi-perpendicular laminar bow shock. *Journal of Geophysical Research*, *80*(4), 502-514. https://doi.org/10.1029/JA080i004p00502

Goncharov, O., Šafránková, J., Němeček, Z., Přech, L., Pitňa, A., & Zastenker, G. N. (2014). Upstream and downstream wave packets associated with low-Mach number interplanetary shocks. *Geophysical Research Letters*, *41*(22), 8100-8106. https://doi.org/10.1002/2014GL062149

Hobara, Y., Balikhin, M., Krasnoselskikh, V., Gedalin, M., & Yamagishi, H. (2010). Statistical study of the quasi - perpendicular shock ramp widths. *Journal of Geophysical Research: Space Physics*, *115*(A11). https://doi.org/10.1029/2010JA015659

Kennel, C. F. (1994, August). The magnetohydrodynamic Rankine-Hugoniot relations. In *AIP Conference Proceedings* (Vol. 314, No. 1, pp. 180-227). American Institute of Physics. https://doi.org/10.1063/1.46750

Liu, Y., Richardson, J. D., & Belcher, J. W. (2005). A statistical study of the properties of interplanetary coronal mass ejections from 0.3 to 5.4 AU. *Planetary and Space Science*, *53*(1-3), 3-17. https://doi.org/10.1016/j.pss.2004.09.023

Lepping, R. P., & Argentiero, P. D. (1971). Single spacecraft method of estimating shock normals. *Journal of Geophysical Research*, *76*(19), 4349-4359. https://doi.org/10.1029/JA076i019p04349

Le, G., Chi, P. J., Blanco-Cano, X., Boardsen, S., Slavin, J. A., Anderson, B. J., & Korth, H. (2013). Upstream ultra-low frequency waves in Mercury's foreshock region: MESSENGER magnetic field observations. *Journal of Geophysical Research: Space Physics*, *118*(6), 2809-2823. https://doi.org /10.1002/jgra.50342

Masters, A., Slavin, J. A., DiBraccio, G. A., Sundberg, T., Winslow, R. M., Johnson, C. L., ... & Korth, H. (2013). A comparison of magnetic overshoots at the bow shocks of Mercury and Saturn. *Journal of Geophysical Research: Space Physics*, *118*(7), 4381-4390. https://doi.org/10.1002/jgra.50428

Mellott, M. M., & Greenstadt, E. W. (1984). The structure of oblique subcritical bow shocks: ISEE 1 and 2 observations. *Journal of Geophysical Research: Space Physics*, *89*(A4), 2151-2161. https://doi.org/10.1029/JA089iA04p02151

Oka, M., Wilson III, L. B., Phan, T. D., Hull, A. J., Amano, T., Hoshino, M., ... & Lindqvist, P. A. (2017). Electron scattering by high-frequency whistler waves at earth's bow shock. *The Astrophysical Journal Letters*, *842*(2), L11. https://doi.org/10.3847/2041-8213/aa7759

Oka, M., Otsuka, F., Matsukiyo, S., Wilson, L. B., Argall, M. R., Amano, T., ... & Lindqvist, P. A. (2019). Electron scattering by low-frequency Whistler waves at Earth's bow shock. *The Astrophysical Journal*, *886*(1), 53. https://doi.org/10.3847/1538-4357/ab4a81

Orlowski, D. S., & Russell, C. T. (1991). Ulf waves upstream of the Venus bow shock: Properties of one-hertz waves. *Journal of Geophysical Research: Space Physics*, *96*(A7), 11271-11282. https://doi.org/10.1029/91JA01103

Perez, J. K., & Northrop, T. G. (1970). Stationary waves produced by the earth's bow shock. *Journal of Geophysical Research*, *75*(31), 6011-6023.

https://doi.org/10.1029/JA075i031p06011

Ruhunusiri, S., Halekas, J. S., Espley, J. R., Eparvier, F., Brain, D., Mazelle, C., .& Sulaiman, A. H. (2018). One-hertz waves at Mars: MAVEN observations. *Journal of Geophysical Research: Space Physics*, *123*(5), 3460-3476. https://doi.org/10.1029/2017JA024618

Russell, C. T., & Farris, M. H. (1995). Ultra low frequency waves at the Earth's bow shock. *Advances in Space Research*, *15*(8-9), 285-296. https://doi.org/10.1016/0273-1177(94)00108-D

Russell, C. T. (2007). Upstream whistler-mode waves at planetary bow shocks: A brief review. *Journal of atmospheric and solar-terrestrial physics*, *69*(14), 1739-1746. https://doi.org/10.1016/j.jastp.2006.11.004

Sarantos, M., & Slavin, J. A. (2009). On the possible formation of Alfvén wings at Mercury during encounters with coronal mass ejections. *Geophysical research letters*, *36*(4). https://doi.org/10.1029/2008GL036747

Slavin, J. A., & Holzer, R. E. (1981). Solar wind flow about the terrestrial planets 1. Modeling bow shock position and shape. *Journal of Geophysical Research: Space Physics*, *86*(A13), 11401-11418. https://doi.org/10.1029/JA086iA13p11401

Slavin, J. A., DiBraccio, G. A., Gershman, D. J., Imber, S. M., Poh, G. K., Raines, J. M., ... & Solomon, S. C. (2014). MESSENGER observations of Mercury's dayside magnetosphere under extreme solar wind conditions. *Journal of Geophysical Research: Space Physics*, *119*(10), 8087-8116. https://doi.org/10.1002/2014JA020319

Slavin, J. A., Middleton, H. R., Raines, J. M., Jia, X., Zhong, J., Sun, W. J., ... & Mays, M. L. (2019). MESSENGER observations of disappearing dayside magnetosphere events at Mercury. *Journal of Geophysical Research: Space Physics*, *124*(8), 6613-6635. https://doi.org/10.1029/2019JA026892

Sonnerup, B. Ö., & Cahill Jr, L. J. (1967). Magnetopause structure and attitude from Explorer 12 observations. *Journal of Geophysical Research*, *72*(1), 171-183. https://doi.org/10.1029/JZ072i001p00171

Sulaiman, A. H., Gurnett, D. A., Halekas, J. S., Yates, J. N., Kurth, W. S., & Dougherty, M. K. (2017). Whistler mode waves upstream of Saturn. *Journal of Geophysical Research: Space Physics*, *122*(1), 227-234. https://doi.org/10.1002/2016JA023501

Tidman, D. A., & Krall, N. A. (1971). Shock Waves in Collisionless Plasmas (New York: Wiley Interscience). *and*, *151*, 135.

Wilson, L. B. (2016). Low frequency waves at and upstream of collisionless shocks. *Washington DC American Geophysical Union Geophysical Monograph Series*, *216*, 269-291. https://doi.org /10.1002/ 9781119055006.ch16

Winslow, R. M., Anderson, B. J., Johnson, C. L., Slavin, J. A., Korth, H., Purucker, M. E., ... & Solomon, S. C. (2013). Mercury's magnetopause and bow shock from MESSENGER Magnetometer observations. *Journal of Geophysical Research: Space Physics*, *118*(5), 2213-2227. https://doi.org/10.1002/jgra.50237

Winslow, R. M., Lugaz, N., Philpott, L. C., Schwadron, N. A., Farrugia, C. J., Anderson, B. J., & Smith, C. W. (2015). Interplanetary coronal mass ejections from MESSENGER orbital observations at Mercury. *Journal of Geophysical Research: Space Physics*, *120*(8), 6101-6118. https://doi.org/10.1002/2015JA021200

Winslow, R. M., Philpott, L., Paty, C. S., Lugaz, N., Schwadron, N. A., Johnson, C. L., & Korth, H. (2017). Statistical study of ICME effects on Mercury's magnetospheric boundaries and nor thern cusp region from MESSENGER. *Journal of Geophysical Research: Space Physics*, *122*(5), 4960-4975. https://doi.org/10.1002/2016JA023548

Winslow, R. M., Lugaz, N., Philpott, L., Farrugia, C. J., Johnson, C. L., Anderson, B. J., ... & Al Asad, M. (2020). Observations of extreme ICME ram pressure compressing Mercury's dayside magnetosphere to the surface. *The Astrophysical Journal*, *889*(2), 184. https://iopscience.iop.org/article/10.3847/1538-4357/ab6170/meta

Zhong, J., Lee, L. C., Wang, X. G., Pu, Z. Y., He, J. S., Wei, Y., & Wan, W. X. (2020). Multiple X-line reconnection observed in Mercury's magnetotail driven by an interplanetary coronal mass ejection. *The Astrophysical Journal Letters*, *893*(1), L11.https://iopscience.iop.org/article/10.3847/2041-8213/ab8566/meta

Geophysical Research Letters

Supporting Information for

MESSENGER Observations of Standing Whistler Waves Upstream of Bow Shock of Mercury

Yang Wang[1,2], Jun Zhong[1,2], James Slavin[3], Hui Zhang [1,2], Lou-Chuang Lee[4,5], Lican Shan[1,2], Yong Wei[1,2], Yongxin Pan[1,2]

[1]Key Laboratory of Earth and Planetary Physics, Institute of Geology and Geophysics, Chinese Academy of Sciences, Beijing, China

[2]College of Earth and Planetary Sciences, University of Chinese Academy of Sciences, Beijing, China

[3]Department of Climate and Space Sciences and Engineering, University of Michigan, Ann Arbor, Michigan, USA

[4]Institute of Earth Sciences, Academia Sinica, Taipei, Taiwan

[5]State Key Laboratory of Lunar and Planetary Sciences, Macau University of Science and Technology, Macau, China

Correspondence to: Jun Zhong (j.zhong@mail.iggcas.ac.cn)

Additional Supporting Information (Files uploaded separately)

1. Caption for Tables S1
2. Caption for Figure S1

Introduction

In file Tables S1, we list some parameters of 36 standing whistler waves, and the description of parameters in each column is as follows:

1. Column "Event", the serial number of the wave events.
2. Column "Start", the start time of the wave events.
3. Column "End", the end time of the wave events.
4. Column "Θbn/°", the angle between upstream magnetic field and shock normal.
5. Column "Θkn/°", the angle between wave vector and shock normal.
6. Column "Θkb/°", the angle between wave vector and upstream magnetic field.
7. Column "Damping ditance/km", the distance from shock along wave vector when amplitude of waves damp to 1/e in the spacecraft coordinate frame (SCF).
8. Column "T_0/Twave", ratio between the time interval T_0 from shock when amplitude of waves damp to 1/e and wave periods in the SCF.
9. Column "Frequency/Hz", the frequency of waves in the SCF.
10. Column "δBwave/Bup", relative wave amplitude: ratio of wave amplitude to upstream magnetic field intensity.
11. Column "Bdown/Bup", ratio of downstream magnetic field intensity to upstream magnetic field intensity.
12. Column "M_A", Alfvén Mach number

In file Figure S1, we compressed all figure of wave events into this file, and the description of every figure as follows:

1. Subgraph "(a)", magnetic field intensity.
2. Subgraph "(b)", component of magnetic field in aberrated Mercury solar magnetic (MSM) coordinates.
3. Subgraph "(c)", component of the magnetic field of wave after removing the background magnetic field in minimum variance analysis (MVA).
4. Subgraph "(d)", the variations of the total power along shock normal in the SCF.
5. Subgraph "(e)", magnetic field of the wave in the maximum-intermediate plane after removing the background magnetic field.
6. Subgraph "(f)", power spectral density of magnetic field after removing the background magnetic field.
7. Subgraph "(g)", location of bow shock in the X-ρ($\sqrt{Y^2+Z^2}$) plane .Black curve is best fit conic section from Winslow et al. (2017) . Black arrow is shock normal. Blue arrow is wave vector.

Event 1

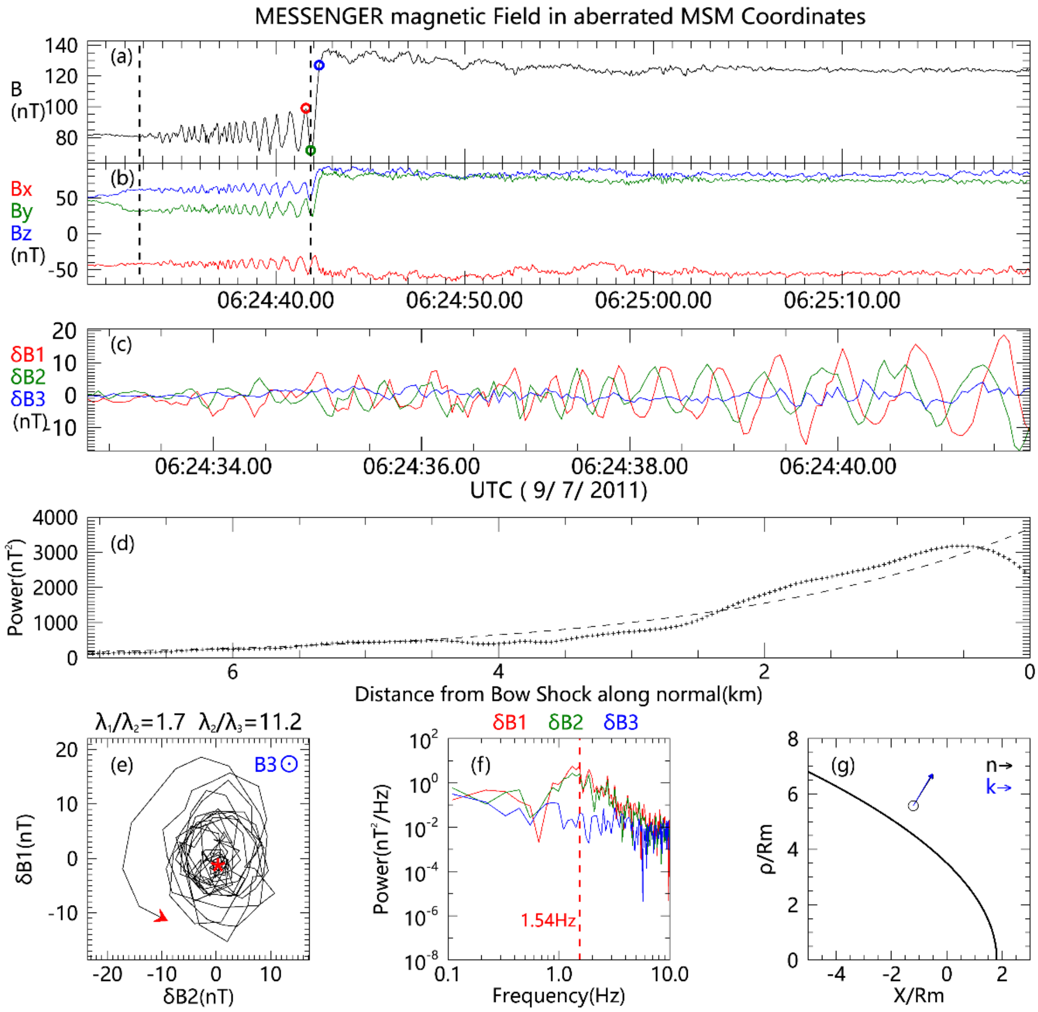

MESSENGER magnetic Field in aberrated MSM Coordinates
(a)
B (nT)
(b)
Bx
By
Bz
(nT)
06:24:40.00
06:24:50.00
06:25:00.00
06:25:10.00
(c)
δB1
δB2
δB3
(nT)
06:24:34.00
06:24:36.00
06:24:38.00
06:24:40.00
UTC (9/ 7/ 2011)
(d)
Power(nT²)
Distance from Bow Shock along normal(km)
λ₁/λ₂=1.7 λ₂/λ₃=11.2
(e)
B3
δB1(nT)
δB2(nT)
(f)
1.54Hz
Power(nT²/Hz)
Frequency(Hz)
(g)
n→
k→
ρ/Rm
X/Rm

Event 2

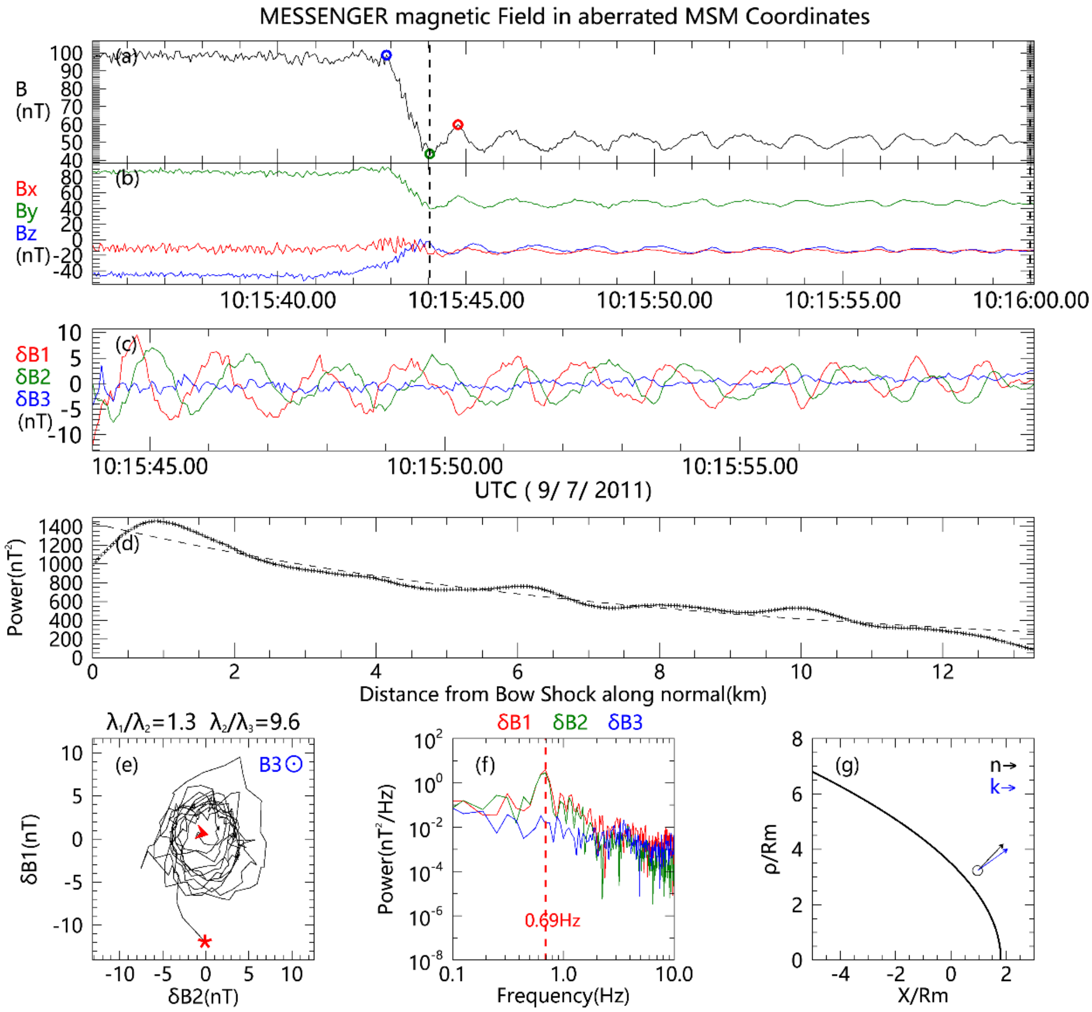

MESSENGER magnetic Field in aberrated MSM Coordinates
(a)
B (nT)
(b)
Bx
By
Bz
(nT)
10:15:40.00
10:15:45.00
10:15:50.00
10:15:55.00
10:16:00.00
(c)
δB1
δB2
δB3
(nT)
10:15:45.00
10:15:50.00
10:15:55.00
UTC (9/ 7/ 2011)
(d)
Power(nT²)
Distance from Bow Shock along normal(km)
λ₁/λ₂=1.3 λ₂/λ₃=9.6
(e)
B3
δB1(nT)
δB2(nT)
(f)
δB1 δB2 δB3
Power(nT²/Hz)
0.69Hz
Frequency(Hz)
(g)
n
k
ρ/Rm
X/Rm

Event 3

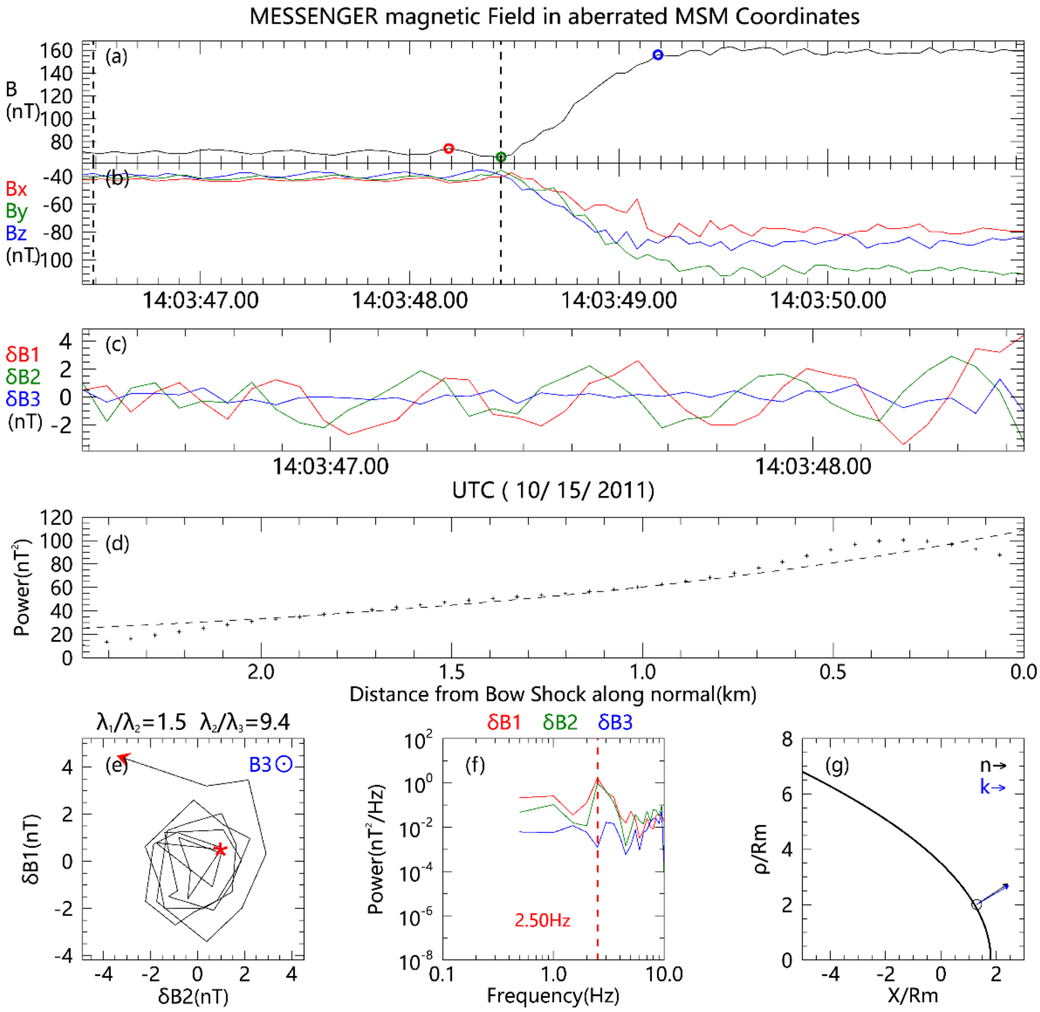

MESSENGER magnetic Field in aberrated MSM Coordinates
(a)
B (nT)
(b)
Bx
By
Bz
(nT)
14:03:47.00
14:03:48.00
14:03:49.00
14:03:50.00
(c)
δB1
δB2
δB3
(nT)
UTC (10/ 15/ 2011)
(d)
Power(nT²)
Distance from Bow Shock along normal(km)
λ1/λ2=1.5 λ2/λ3=9.4
(e)
B3
δB1(nT)
δB2(nT)
(f)
δB1 δB2 δB3
Power(nT²/Hz)
2.50Hz
Frequency(Hz)
(g)
n
k
ρ/Rm
X/Rm

Event 4

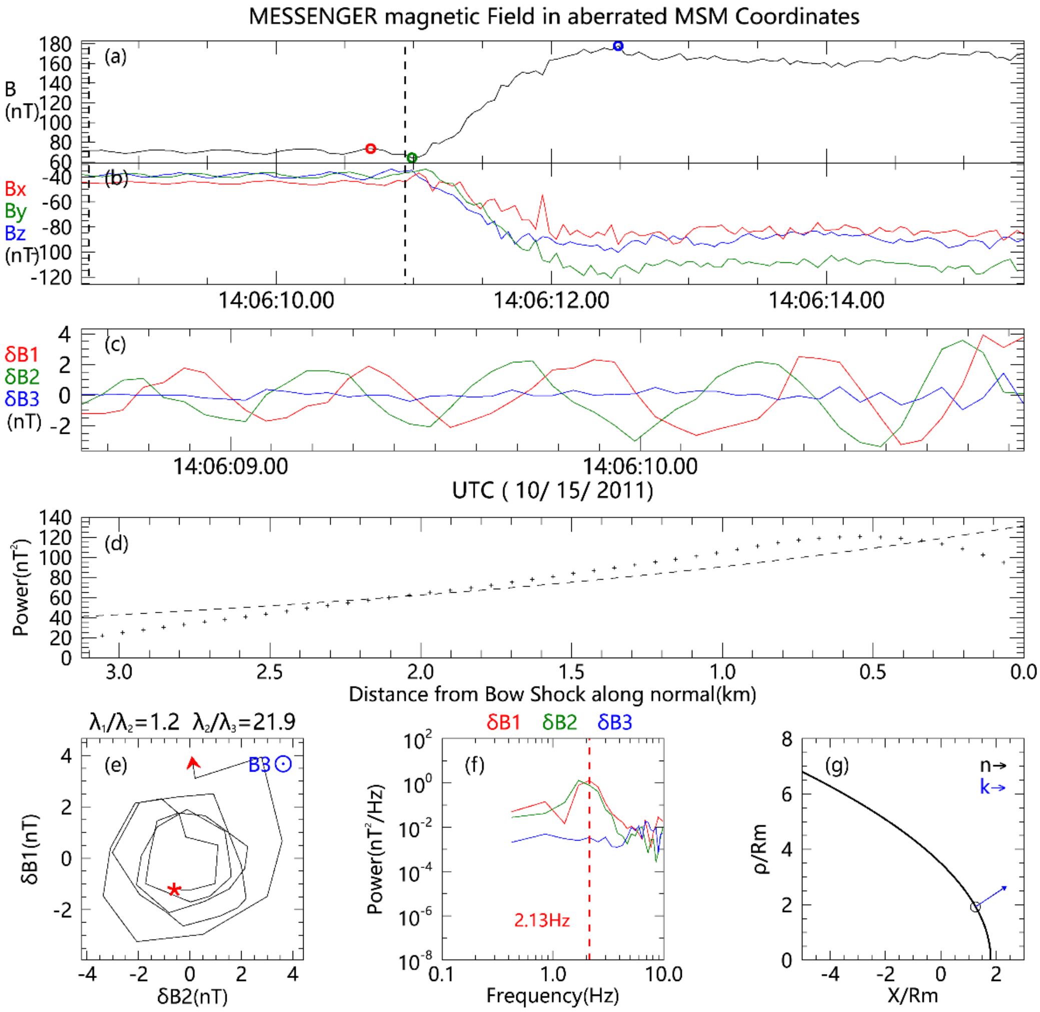

MESSENGER magnetic Field in aberrated MSM Coordinates
(a)
B (nT)
(b)
Bx
By
Bz
(nT)
14:06:10.00
14:06:12.00
14:06:14.00
(c)
δB1
δB2
δB3
(nT)
14:06:09.00
14:06:10.00
UTC (10/ 15/ 2011)
(d)
Power(nT²)
Distance from Bow Shock along normal(km)
λ₁/λ₂=1.2 λ₂/λ₃=21.9
(e)
B3
δB1(nT)
δB2(nT)
δB1 δB2 δB3
(f)
Power(nT²/Hz)
2.13Hz
Frequency(Hz)
(g)
n
k
ρ/Rm
X/Rm

Event 5

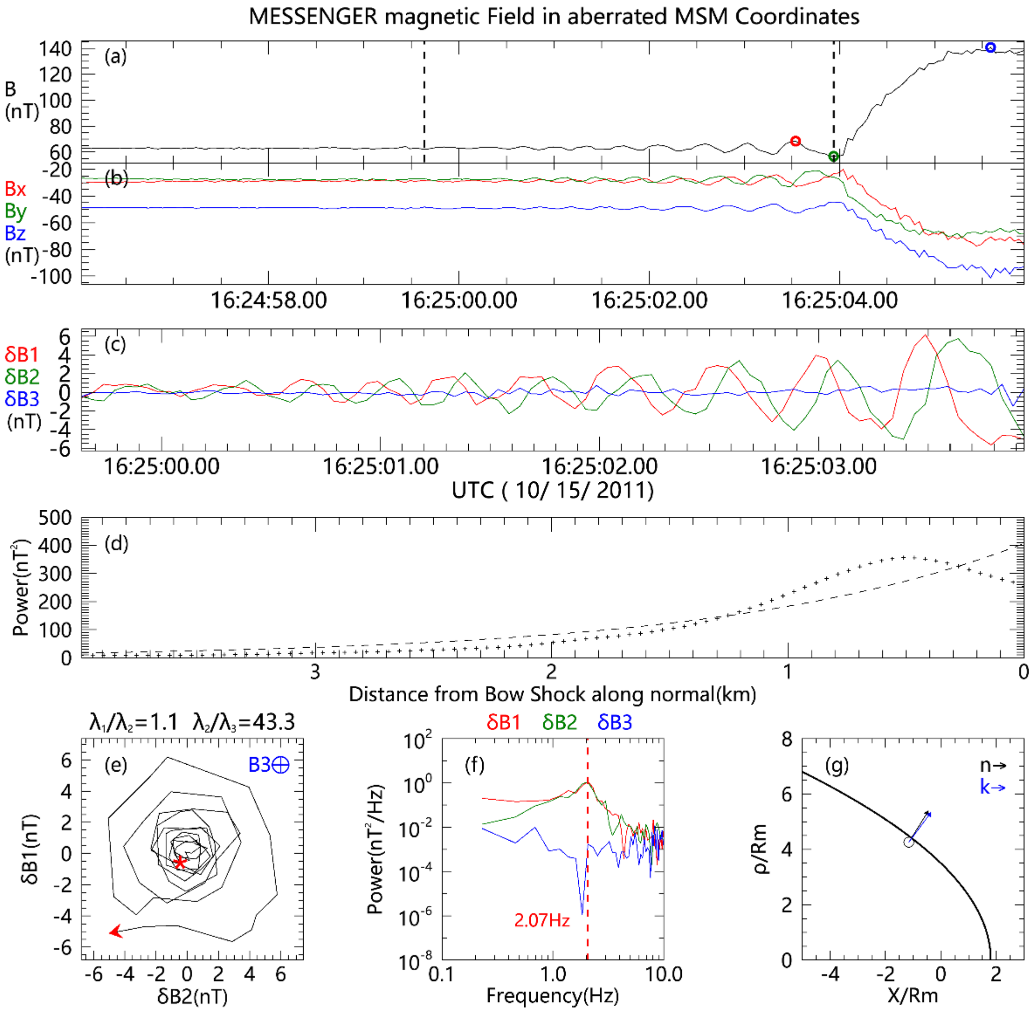

MESSENGER magnetic Field in aberrated MSM Coordinates
(a)
B (nT)
(b)
Bx
By
Bz
(nT)
16:24:58.00
16:25:00.00
16:25:02.00
16:25:04.00
(c)
δB1
δB2
δB3
(nT)
16:25:00.00
16:25:01.00
16:25:02.00
16:25:03.00
UTC (10/ 15/ 2011)
(d)
Power(nT²)
Distance from Bow Shock along normal(km)
λ1/λ2=1.1 λ2/λ3=43.3
(e)
B3⊕
δB1(nT)
δB2(nT)
δB1 δB2 δB3
(f)
Power(nT²/Hz)
2.07Hz
Frequency(Hz)
(g)
n→
k→
ρ/Rm
X/Rm

Event 6

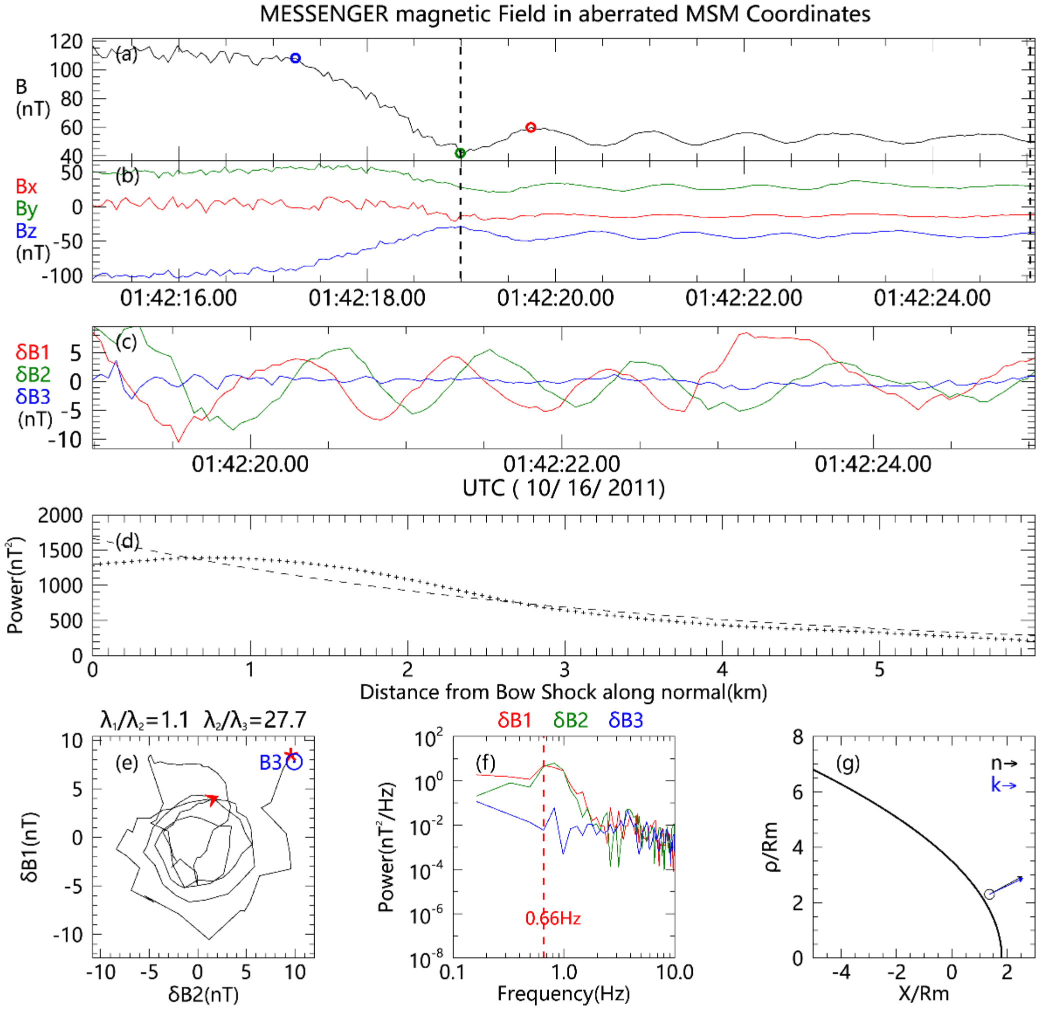

MESSENGER magnetic Field in aberrated MSM Coordinates
(a)
B (nT)
120
100
80
60
40
(b)
Bx
By
Bz
(nT)
50
0
-50
-100
01:42:16.00
01:42:18.00
01:42:20.00
01:42:22.00
01:42:24.00
(c)
δB1
δB2
δB3
(nT)
5
0
-5
-10
01:42:20.00
01:42:22.00
01:42:24.00
UTC (10/ 16/ 2011)
(d)
Power(nT²)
2000
1500
1000
500
0
Distance from Bow Shock along normal(km)
λ₁/λ₂=1.1 λ₂/λ₃=27.7
(e)
B3
δB1(nT)
δB2(nT)
δB1 δB2 δB3
(f)
Power(nT²/Hz)
0.66Hz
Frequency(Hz)
(g)
n
k
ρ/Rm
X/Rm

Event 7

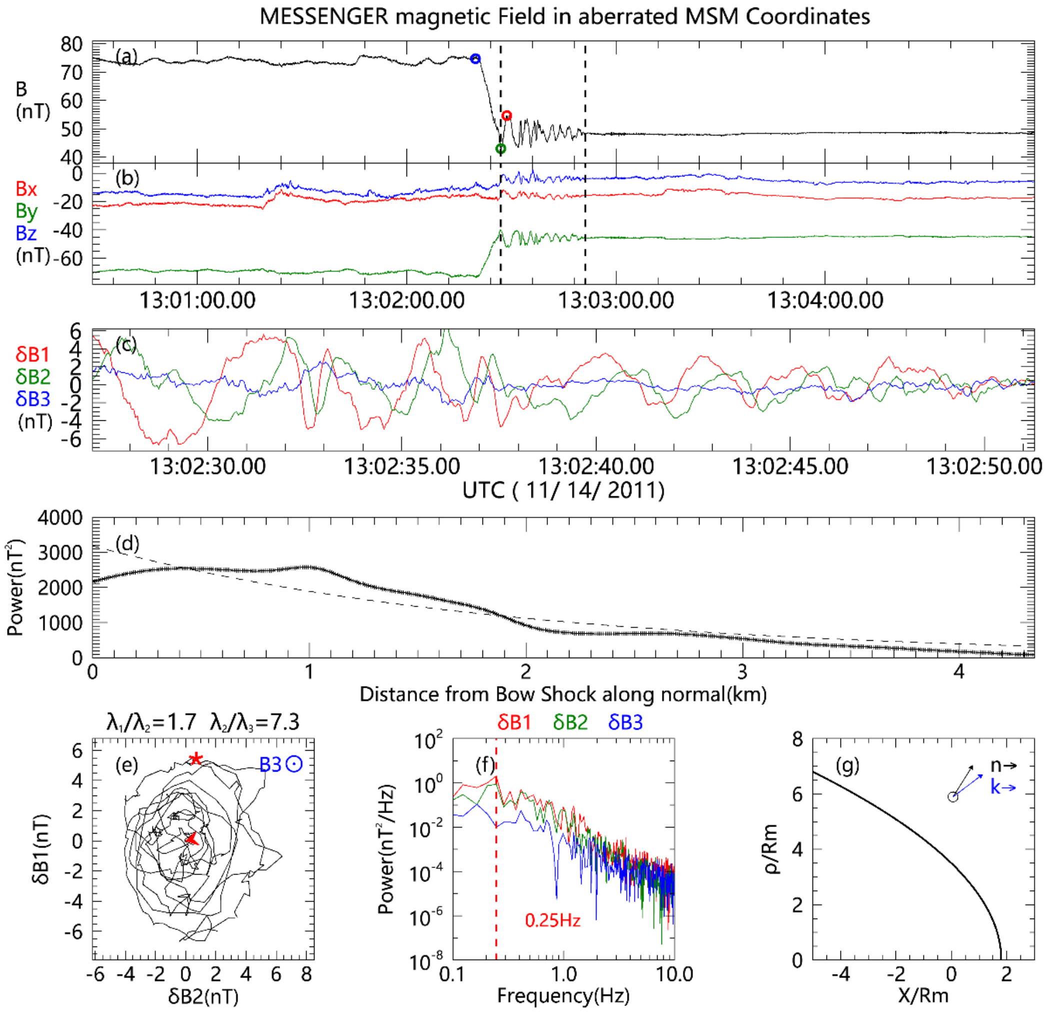

MESSENGER magnetic Field in aberrated MSM Coordinates
(a)
B (nT)
(b)
Bx
By
Bz
(nT)
13:01:00.00
13:02:00.00
13:03:00.00
13:04:00.00
(c)
δB1
δB2
δB3
(nT)
13:02:30.00
13:02:35.00
13:02:40.00
13:02:45.00
13:02:50.00
UTC (11/ 14/ 2011)
(d)
Power(nT²)
Distance from Bow Shock along normal(km)
λ1/λ2=1.7 λ2/λ3=7.3
(e)
B3
δB1(nT)
δB2(nT)
δB1 δB2 δB3
(f)
Power(nT²/Hz)
0.25Hz
Frequency(Hz)
(g)
n→
k→
ρ/Rm
X/Rm

Event 8

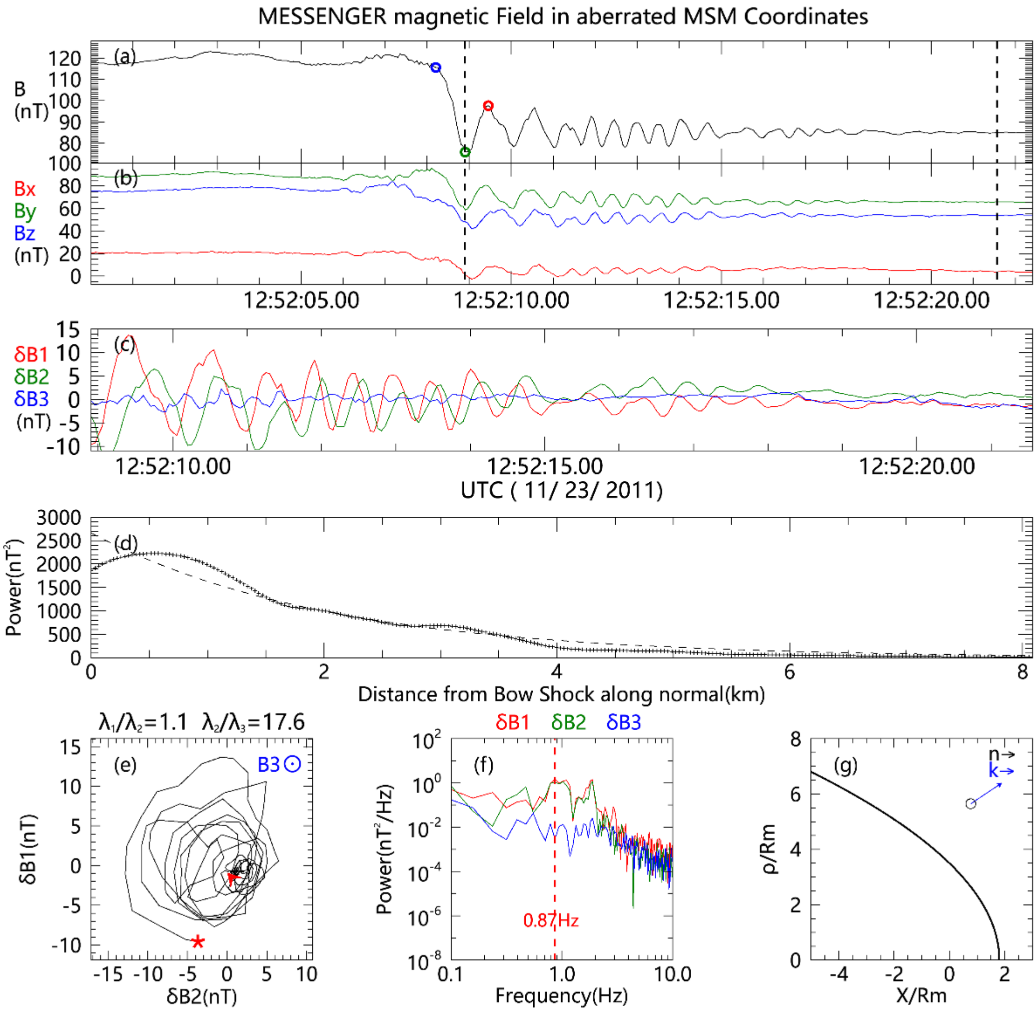

MESSENGER magnetic Field in aberrated MSM Coordinates
(a)
B (nT)
(b)
Bx
By
Bz
(nT)
12:52:05.00
12:52:10.00
12:52:15.00
12:52:20.00
(c)
δB1
δB2
δB3
(nT)
UTC (11/ 23/ 2011)
(d)
Power(nT²)
Distance from Bow Shock along normal(km)
λ₁/λ₂=1.1 λ₂/λ₃=17.6
(e)
B3
δB1(nT)
δB2(nT)
(f)
δB1 δB2 δB3
Power(nT²/Hz)
0.87Hz
Frequency(Hz)
(g)
n
k
ρ/Rm
X/Rm

Event 9

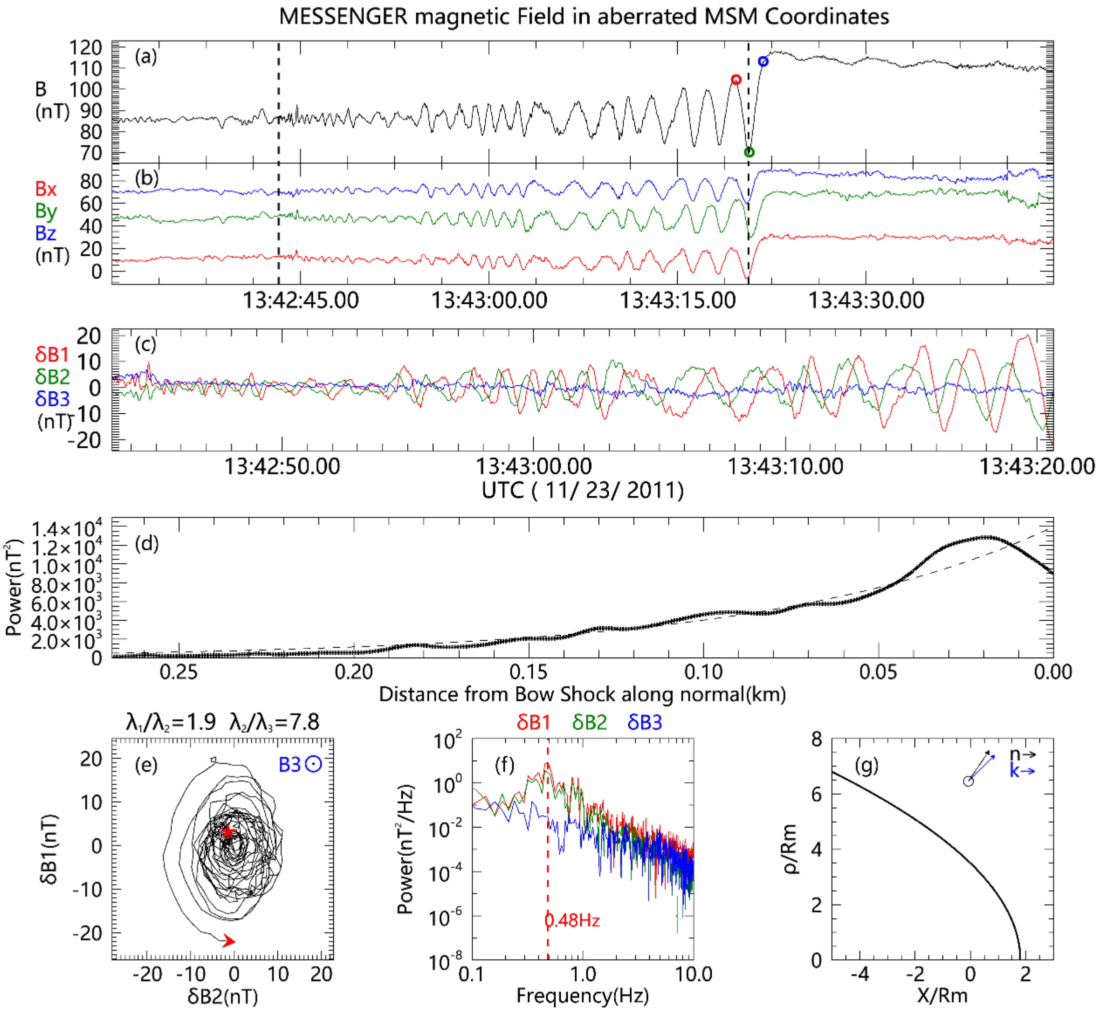

MESSENGER magnetic Field in aberrated MSM Coordinates
(a)
B
(nT)
(b)
Bx
By
Bz
(nT)
13:42:45.00
13:43:00.00
13:43:15.00
13:43:30.00
(c)
δB1
δB2
δB3
(nT)
13:42:50.00
13:43:00.00
13:43:10.00
13:43:20.00
UTC (11/ 23/ 2011)
(d)
Power(nT²)
Distance from Bow Shock along normal(km)
λ₁/λ₂=1.9 λ₂/λ₃=7.8
(e)
B3
δB1(nT)
δB2(nT)
(f)
δB1 δB2 δB3
Power(nT²/Hz)
0.48Hz
Frequency(Hz)
(g)
n
k
ρ/Rm
X/Rm

Event 10

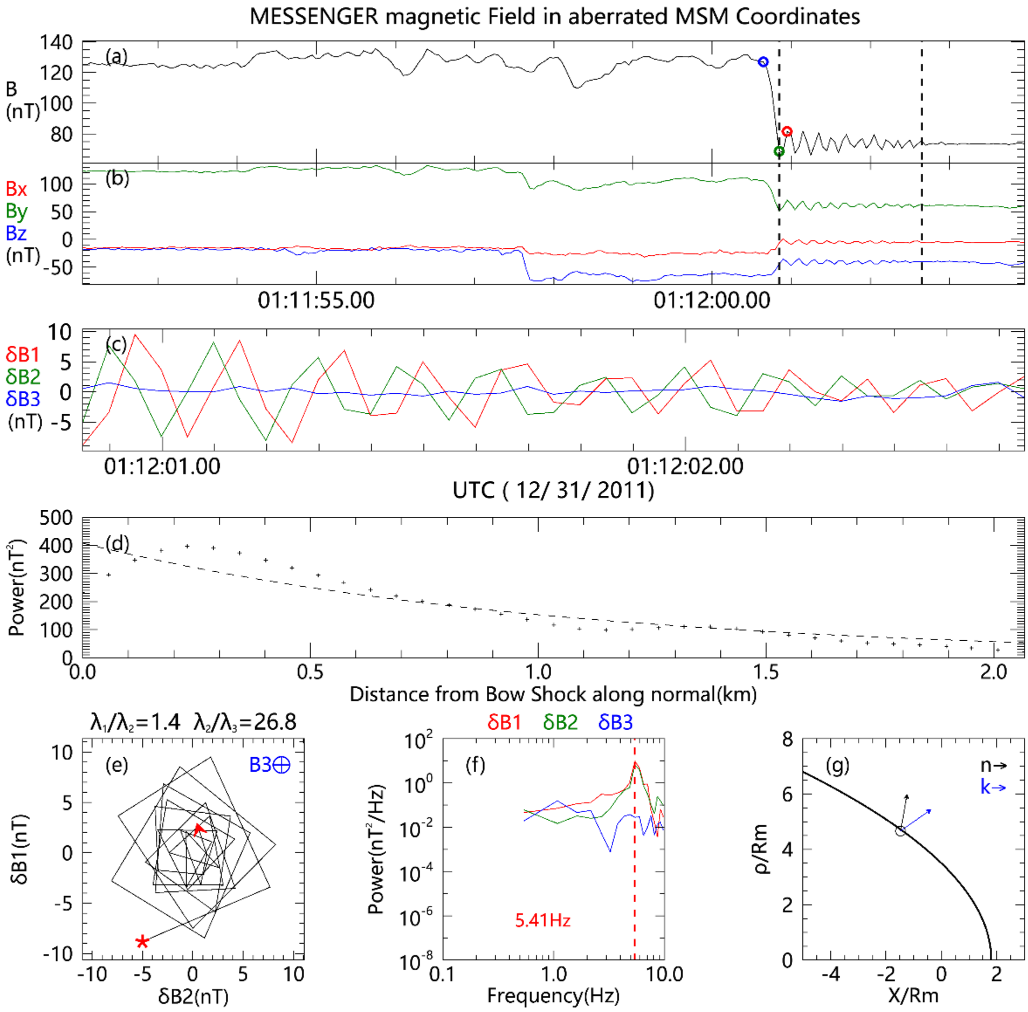

MESSENGER magnetic Field in aberrated MSM Coordinates
(a)
B (nT)
(b)
Bx
By
Bz
(nT)
01:11:55.00
01:12:00.00
(c)
δB1
δB2
δB3
(nT)
01:12:01.00
01:12:02.00
UTC (12/ 31/ 2011)
(d)
Power(nT²)
Distance from Bow Shock along normal(km)
λ₁/λ₂=1.4 λ₂/λ₃=26.8
(e)
B3⊕
δB1(nT)
δB2(nT)
δB1 δB2 δB3
(f)
Power(nT²/Hz)
5.41Hz
Frequency(Hz)
(g)
n→
k→
ρ/Rm
X/Rm

Event 11

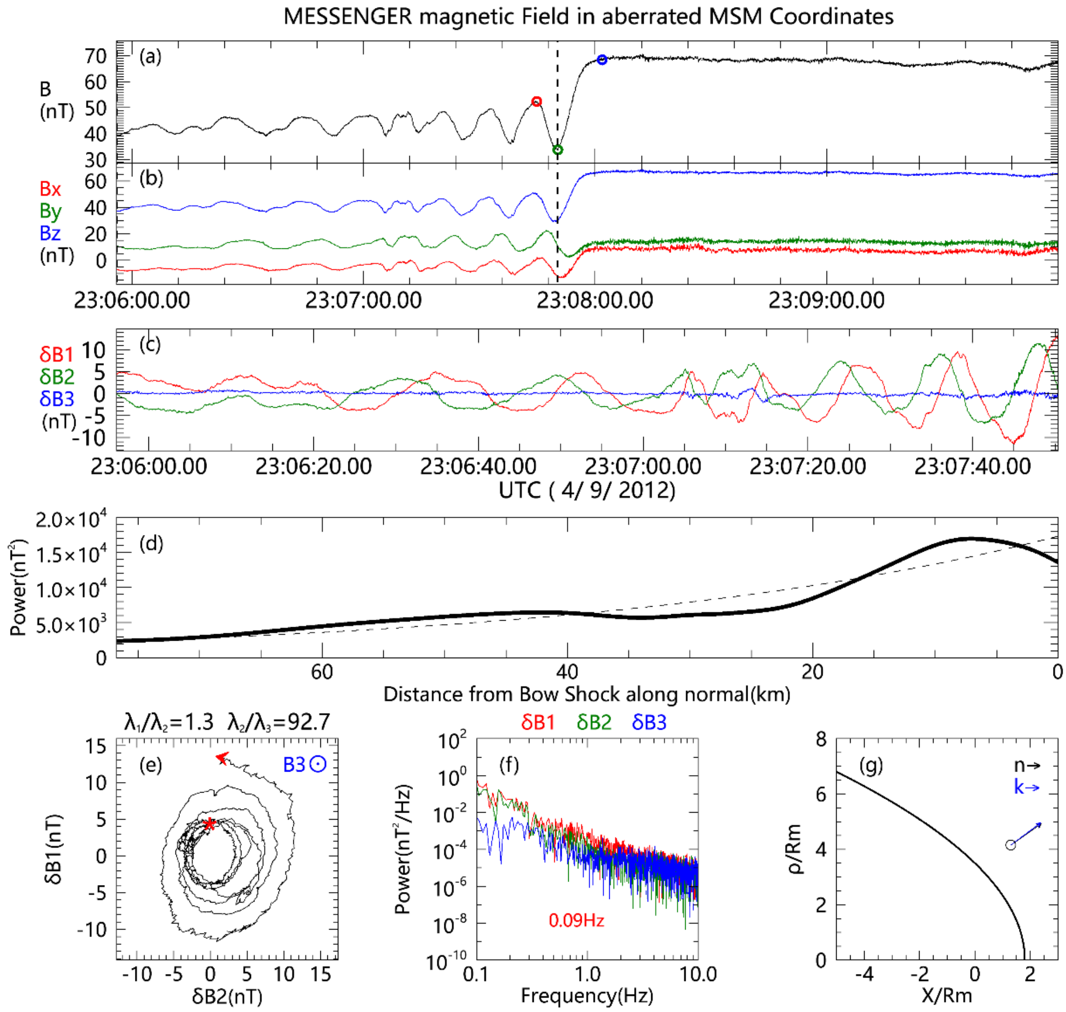

MESSENGER magnetic Field in aberrated MSM Coordinates
(a)
B
(nT)
(b)
Bx
By
Bz
(nT)
23:06:00.00
23:07:00.00
23:08:00.00
23:09:00.00
(c)
δB1
δB2
δB3
(nT)
23:06:20.00
23:06:40.00
23:07:20.00
23:07:40.00
UTC (4/ 9/ 2012)
(d)
Power(nT²)
Distance from Bow Shock along normal(km)
λ1/λ2=1.3 λ2/λ3=92.7
(e)
B3
δB1(nT)
δB2(nT)
δB1 δB2 δB3
(f)
Power(nT²/Hz)
0.09Hz
Frequency(Hz)
(g)
n→
k→
ρ/Rm
X/Rm

Event 12

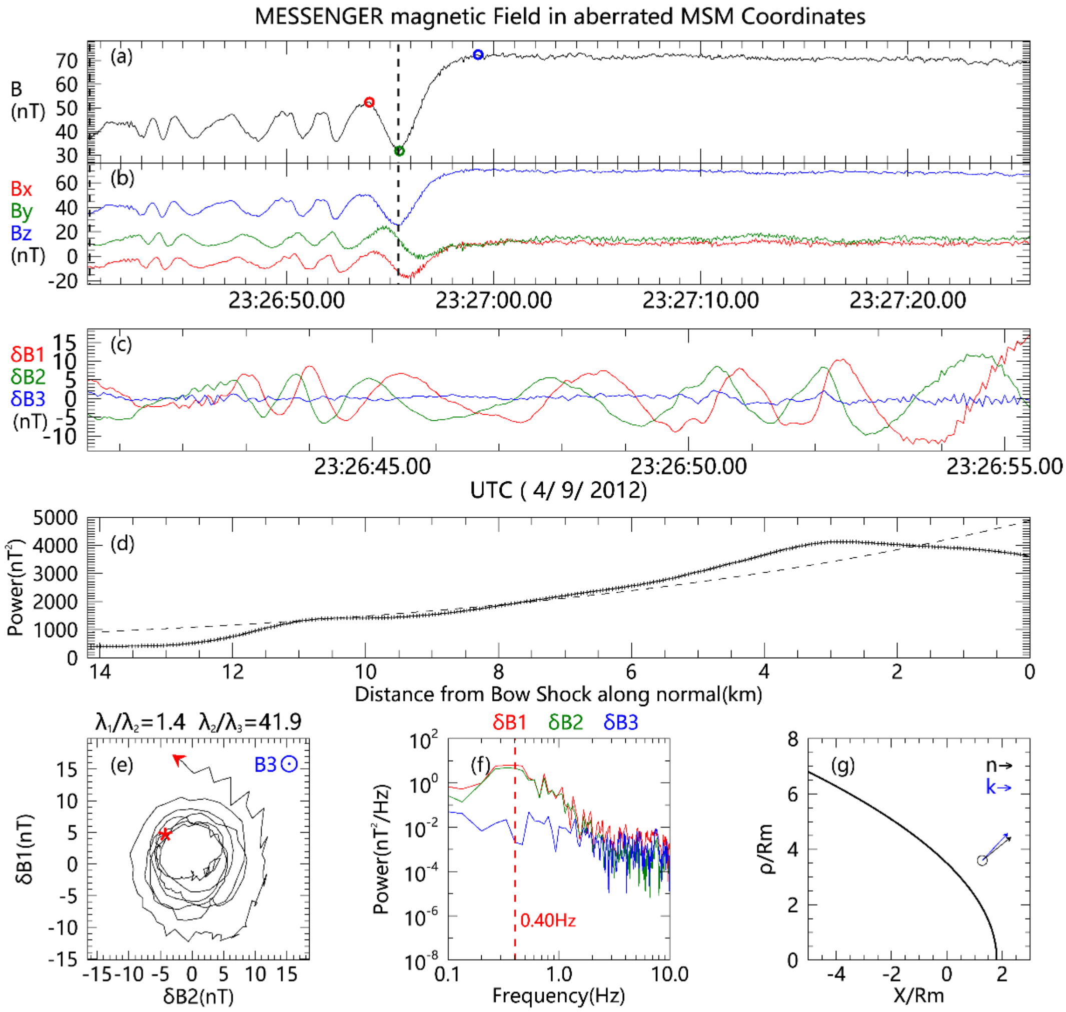
MESSENGER magnetic Field in aberrated MSM Coordinates
(a)
B (nT)
(b)
Bx
By
Bz
(nT)
23:26:50.00
23:27:00.00
23:27:10.00
23:27:20.00
(c)
δB1
δB2
δB3
(nT)
23:26:45.00
23:26:50.00
23:26:55.00
UTC (4/ 9/ 2012)
(d)
Power(nT²)
Distance from Bow Shock along normal(km)
λ₁/λ₂=1.4 λ₂/λ₃=41.9
(e)
B3
δB1(nT)
δB2(nT)
(f)
δB1 δB2 δB3
Power(nT²/Hz)
0.40Hz
Frequency(Hz)
(g)
n
k
ρ/Rm
X/Rm

Event 13

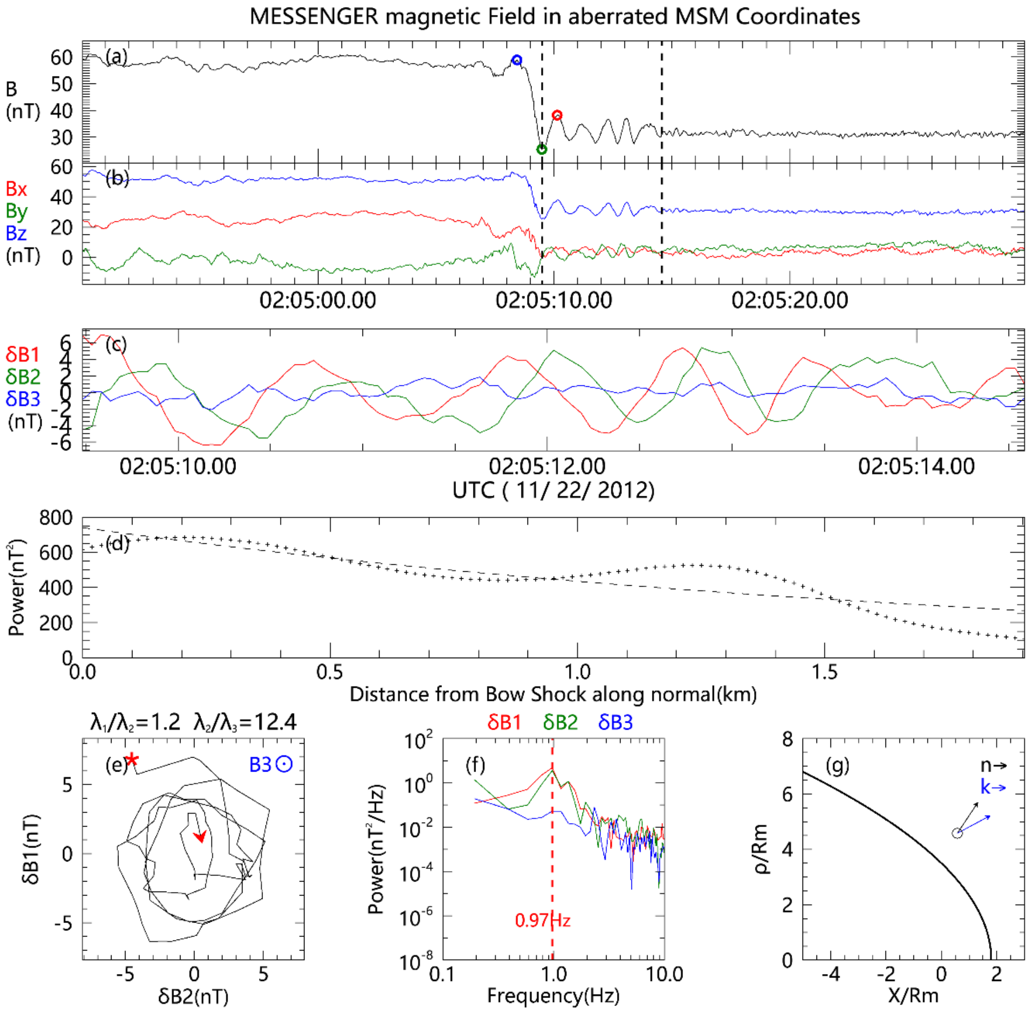
MESSENGER magnetic Field in aberrated MSM Coordinates
(a)
B (nT)
(b)
Bx
By
Bz
(nT)
02:05:00.00
02:05:10.00
02:05:20.00
(c)
δB1
δB2
δB3
(nT)
02:05:10.00
02:05:12.00
02:05:14.00
UTC (11/ 22/ 2012)
(d)
Power(nT²)
Distance from Bow Shock along normal(km)
λ1/λ2=1.2 λ2/λ3=12.4
(e)
B3
δB1(nT)
δB2(nT)
(f)
δB1 δB2 δB3
Power(nT²/Hz)
0.97Hz
Frequency(Hz)
(g)
n
k
ρ/Rm
X/Rm

Event 14

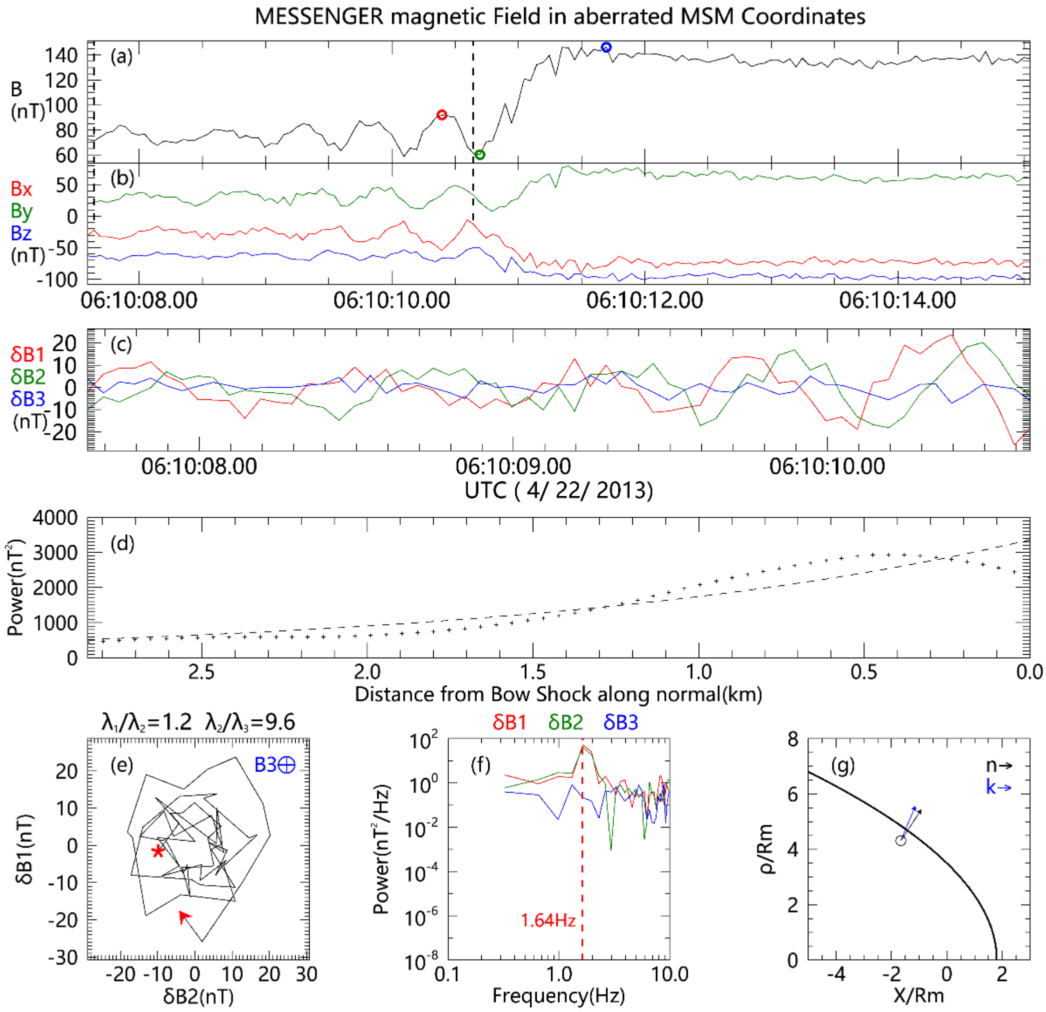

MESSENGER magnetic Field in aberrated MSM Coordinates
(a)
B (nT)
140
120
100
80
60
(b)
Bx
By
Bz
(nT)
50
0
-50
-100
06:10:08.00
06:10:10.00
06:10:12.00
06:10:14.00
(c)
δB1
δB2
δB3
(nT)
20
10
0
-10
-20
06:10:08.00
06:10:09.00
06:10:10.00
UTC (4/ 22/ 2013)
(d)
Power(nT²)
4000
3000
2000
1000
0
2.5
2.0
1.5
1.0
0.5
0.0
Distance from Bow Shock along normal(km)
λ₁/λ₂=1.2 λ₂/λ₃=9.6
(e)
B3⊕
δB1(nT)
δB2(nT)
δB1 δB2 δB3
(f)
Power(nT²/Hz)
1.64Hz
Frequency(Hz)
(g)
n→
k→
ρ/Rm
X/Rm

Event 15

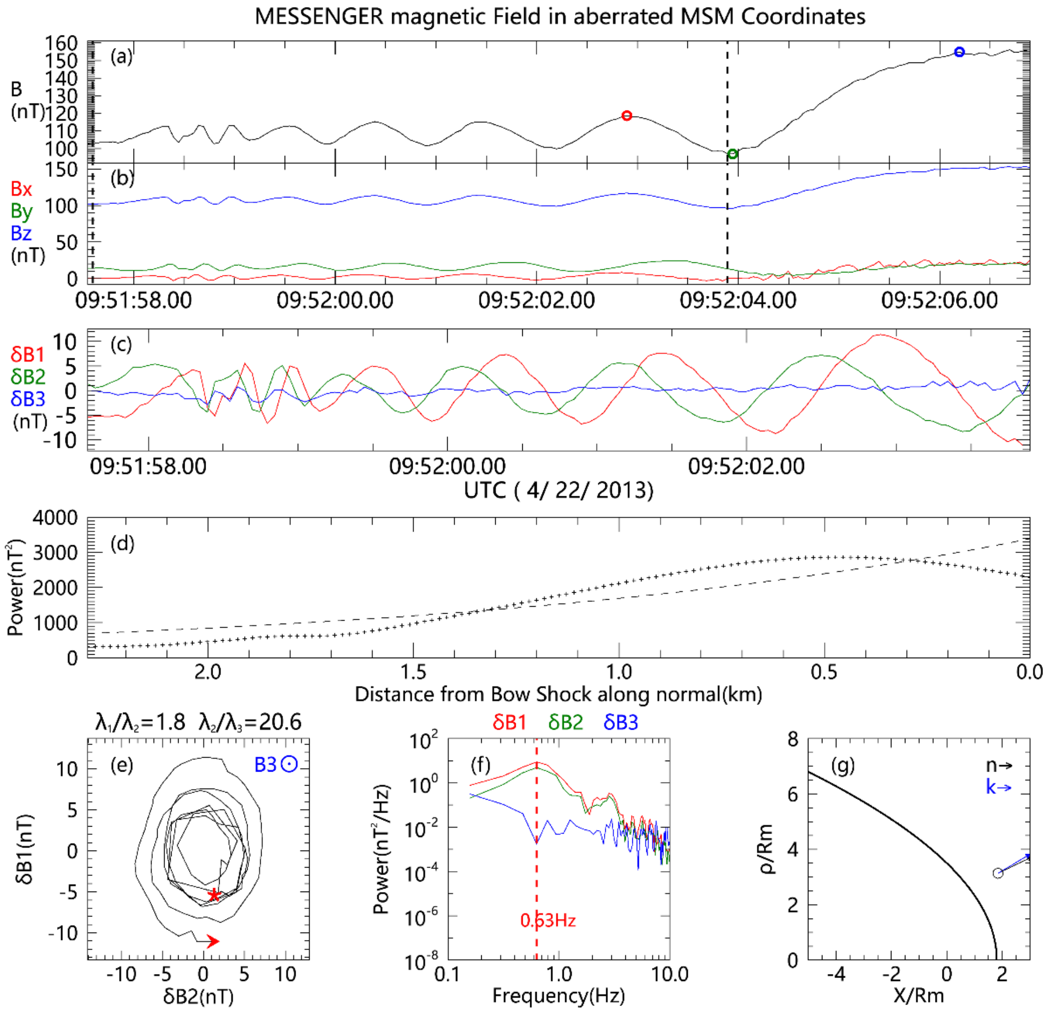

MESSENGER magnetic Field in aberrated MSM Coordinates
(a)
B (nT)
(b)
Bx
By
Bz
(nT)
09:51:58.00
09:52:00.00
09:52:02.00
09:52:04.00
09:52:06.00
(c)
δB1
δB2
δB3
(nT)
UTC (4/ 22/ 2013)
(d)
Power(nT²)
Distance from Bow Shock along normal(km)
λ₁/λ₂=1.8 λ₂/λ₃=20.6
(e)
B3
δB1(nT)
δB2(nT)
(f)
Power(nT²/Hz)
0.63Hz
Frequency(Hz)
(g)
n→
k→
ρ/Rm
X/Rm

Event 16

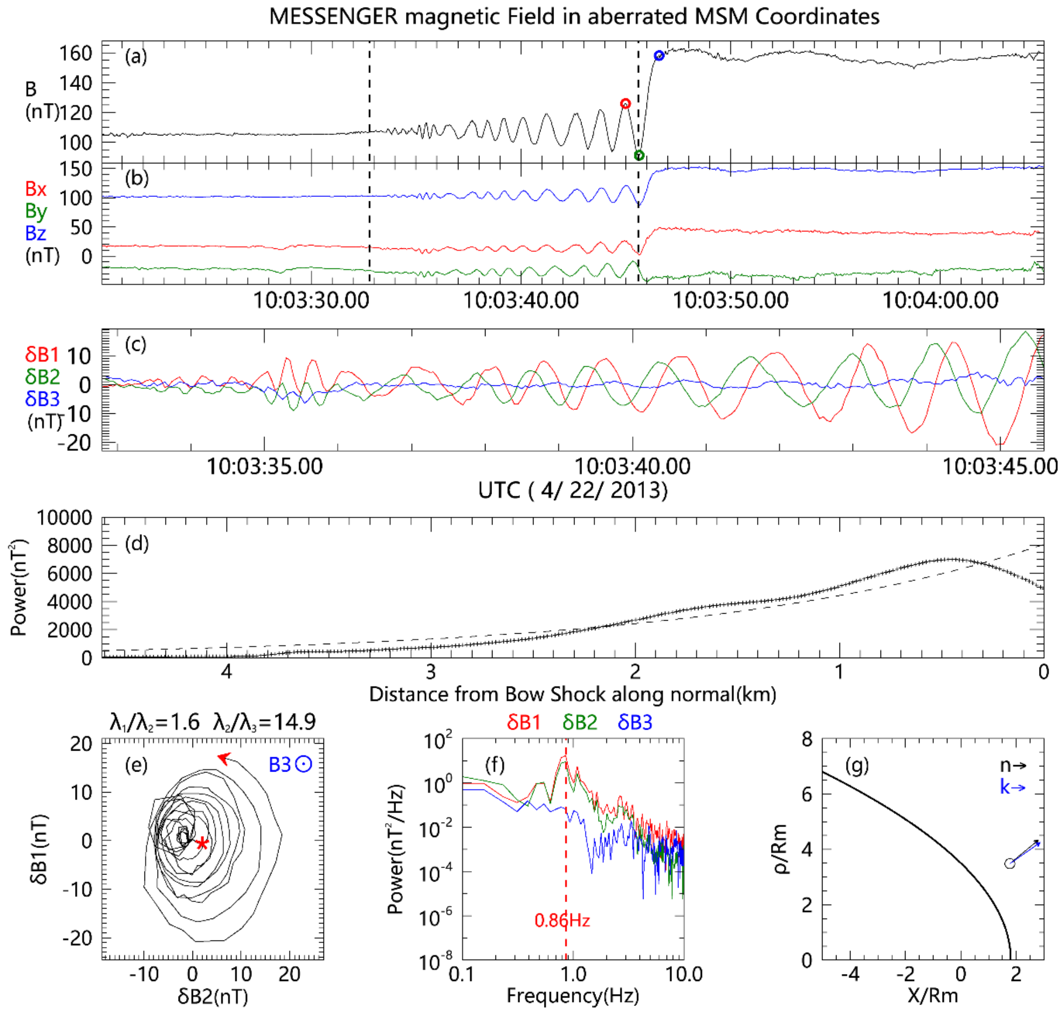

MESSENGER magnetic Field in aberrated MSM Coordinates
(a)
B (nT)
(b)
Bx
By
Bz
(nT)
10:03:30.00
10:03:40.00
10:03:50.00
10:04:00.00
(c)
δB1
δB2
δB3
(nT)
10:03:35.00
10:03:40.00
10:03:45.00
UTC (4/ 22/ 2013)
(d)
Power(nT²)
Distance from Bow Shock along normal(km)
λ₁/λ₂=1.6 λ₂/λ₃=14.9
(e)
B3
δB1(nT)
δB2(nT)
δB1 δB2 δB3
(f)
Power(nT²/Hz)
0.86Hz
Frequency(Hz)
(g)
n
k
ρ/Rm
X/Rm

Event 17

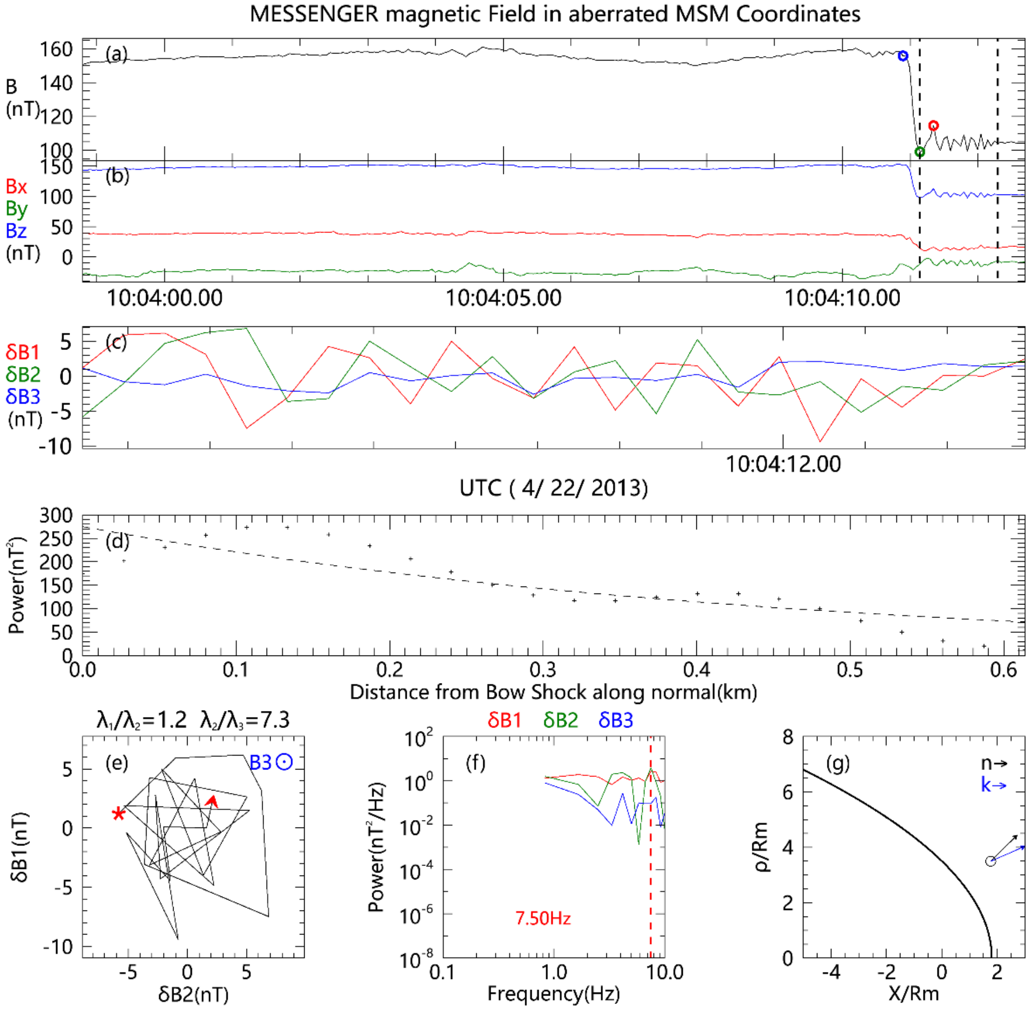

MESSENGER magnetic Field in aberrated MSM Coordinates
(a)
B (nT)
160
140
120
100
(b)
Bx
By
Bz
(nT)
150
100
50
0
10:04:00.00
10:04:05.00
10:04:10.00
(c)
δB1
δB2
δB3
(nT)
5
0
-5
-10
10:04:12.00
UTC (4/ 22/ 2013)
(d)
Power(nT²)
300
250
200
150
100
50
0
0.0
0.1
0.2
0.3
0.4
0.5
0.6
Distance from Bow Shock along normal(km)
λ₁/λ₂=1.2 λ₂/λ₃=7.3
(e)
B3⊙
δB1(nT)
δB2(nT)
(f)
δB1 δB2 δB3
Power(nT²/Hz)
7.50Hz
Frequency(Hz)
0.1
1.0
10.0
(g)
n→
k→
ρ/Rm
X/Rm
8
6
4
2
0
-4
-2
0
2

Event 18

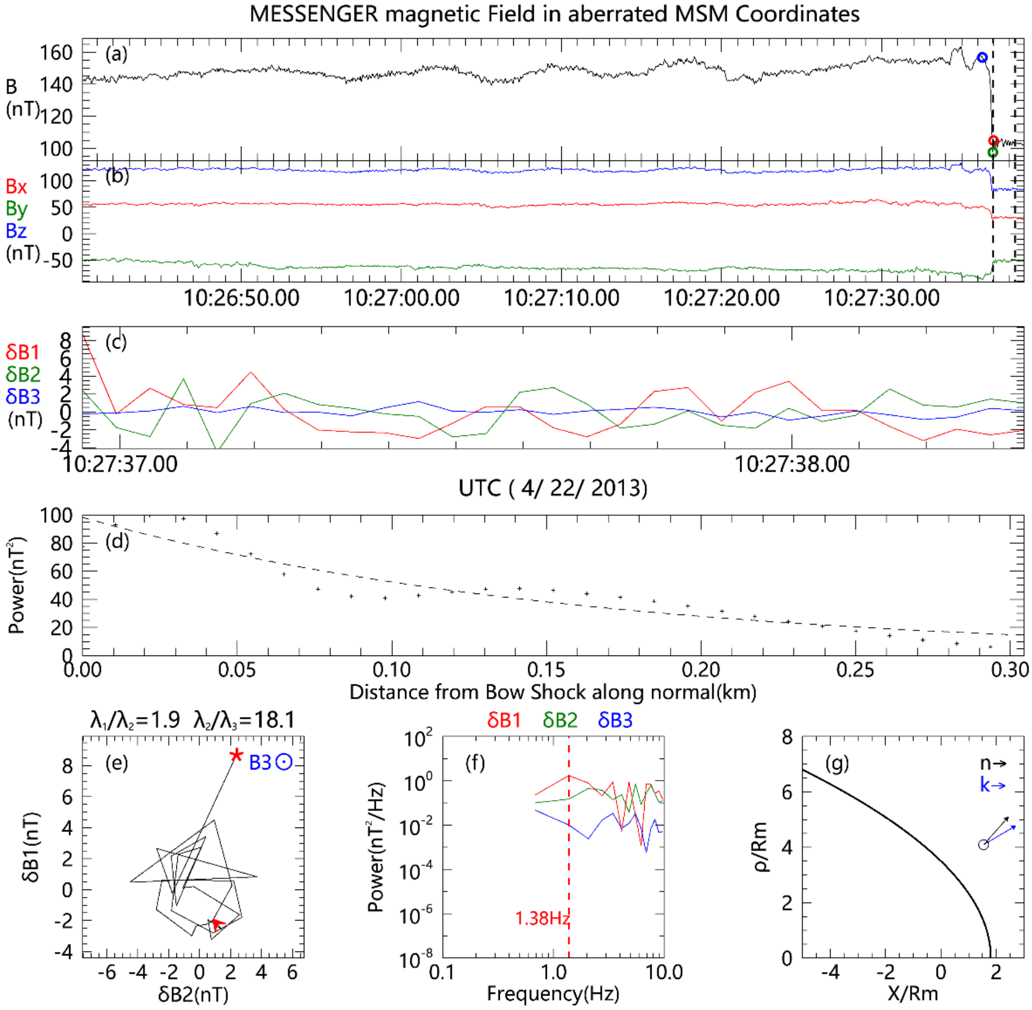

MESSENGER magnetic Field in aberrated MSM Coordinates
B (nT)
Bx
By
Bz
(nT)
10:26:50.00
10:27:00.00
10:27:10.00
10:27:20.00
10:27:30.00
δB1
δB2
δB3
(nT)
10:27:37.00
10:27:38.00
UTC (4/ 22/ 2013)
Power(nT²)
Distance from Bow Shock along normal(km)
λ1/λ2=1.9 λ2/λ3=18.1
B3
δB1(nT)
δB2(nT)
Power(nT²/Hz)
1.38Hz
Frequency(Hz)
ρ/Rm
X/Rm
n
k

Event 19

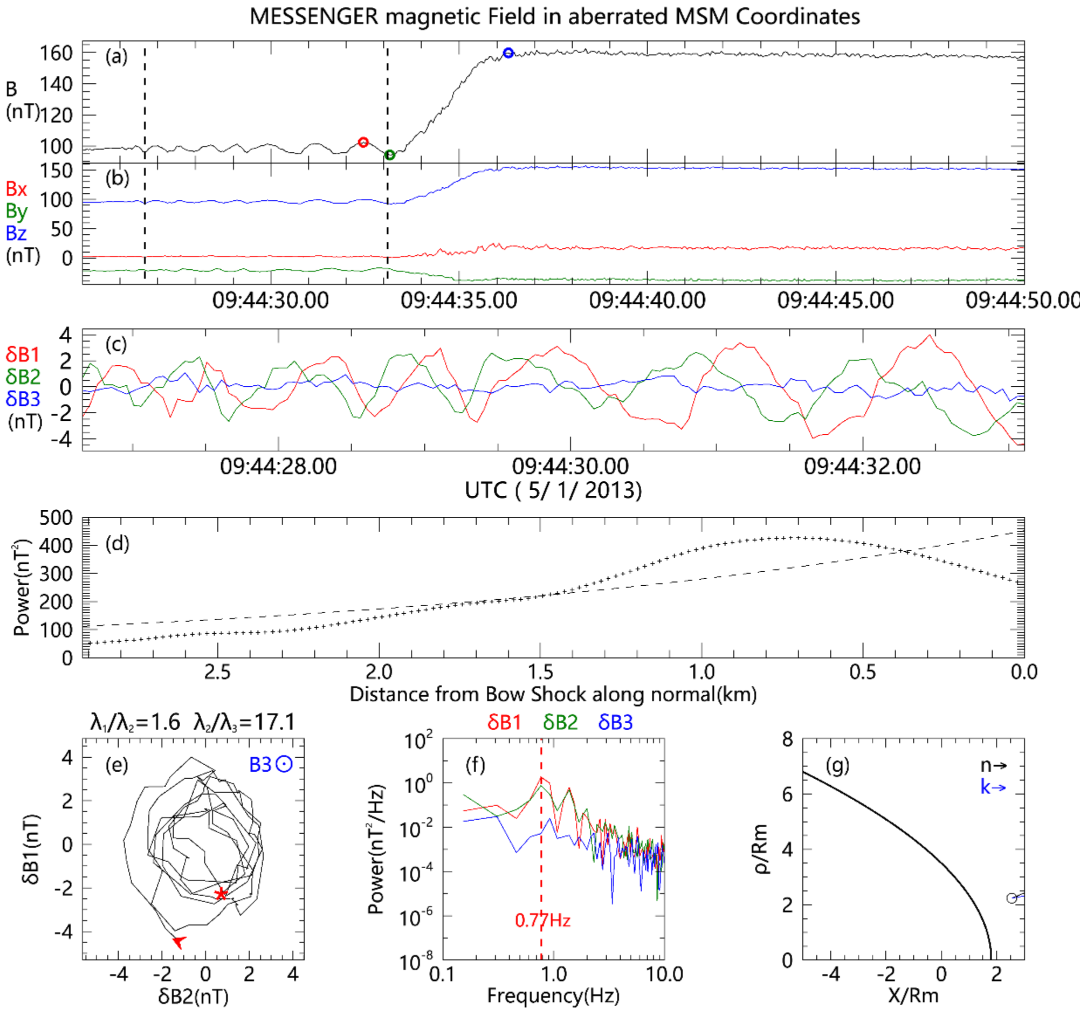

MESSENGER magnetic Field in aberrated MSM Coordinates
(a)
B (nT)
(b)
Bx
By
Bz
(nT)
09:44:30.00
09:44:35.00
09:44:40.00
09:44:45.00
09:44:50.00
(c)
δB1
δB2
δB3
(nT)
09:44:28.00
09:44:30.00
09:44:32.00
UTC (5/ 1/ 2013)
(d)
Power(nT²)
Distance from Bow Shock along normal(km)
λ₁/λ₂=1.6 λ₂/λ₃=17.1
(e)
B3
δB1(nT)
δB2(nT)
(f)
δB1 δB2 δB3
0.77Hz
Power(nT²/Hz)
Frequency(Hz)
(g)
n→
k→
ρ/Rm
X/Rm

Event 20

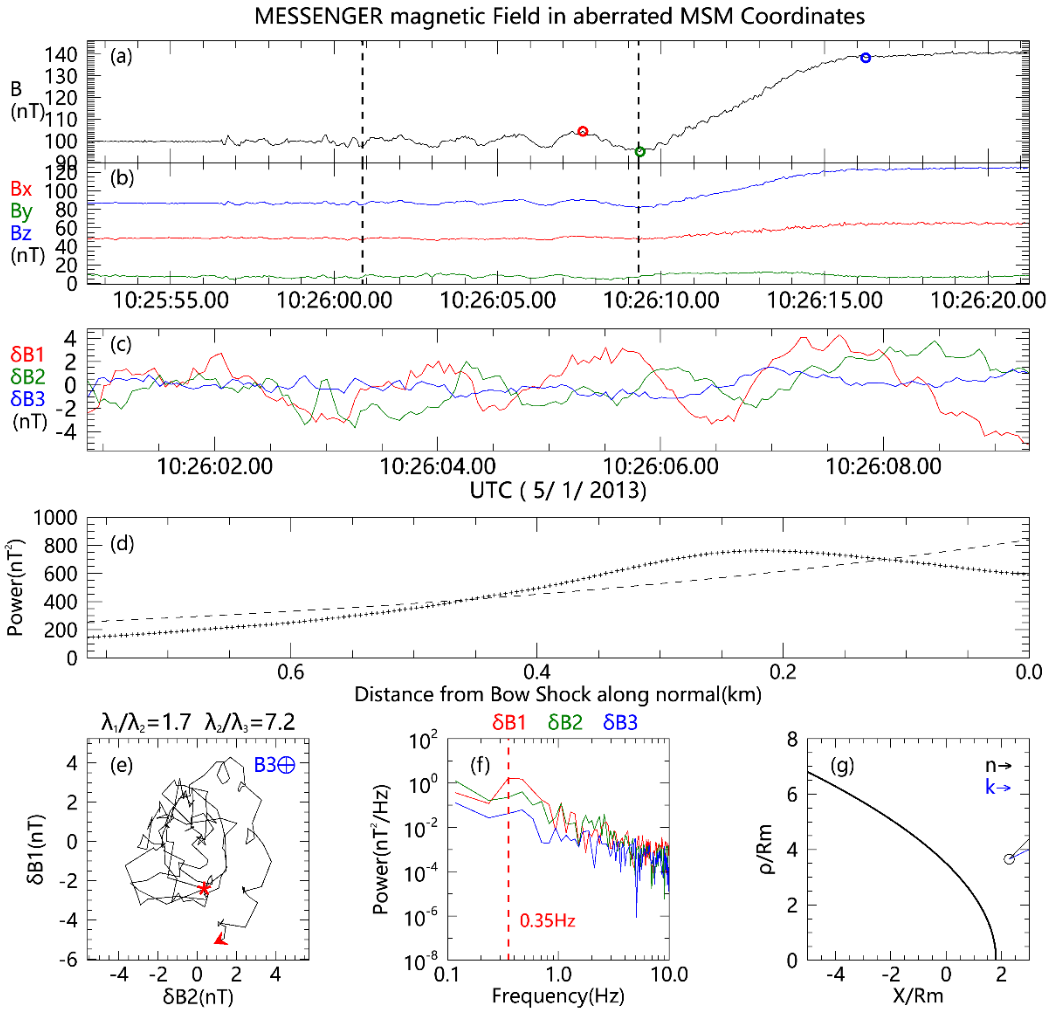

MESSENGER magnetic Field in aberrated MSM Coordinates
(a)
B (nT)
(b)
Bx
By
Bz
(nT)
10:25:55.00
10:26:00.00
10:26:05.00
10:26:10.00
10:26:15.00
10:26:20.00
(c)
δB1
δB2
δB3
(nT)
10:26:02.00
10:26:04.00
10:26:06.00
10:26:08.00
UTC (5/ 1/ 2013)
(d)
Power(nT²)
Distance from Bow Shock along normal(km)
λ₁/λ₂=1.7 λ₂/λ₃=7.2
(e)
B3⊕
δB1(nT)
δB2(nT)
(f)
δB1 δB2 δB3
Power(nT²/Hz)
0.35Hz
Frequency(Hz)
(g)
n→
k→
ρ/Rm
X/Rm

Event 21

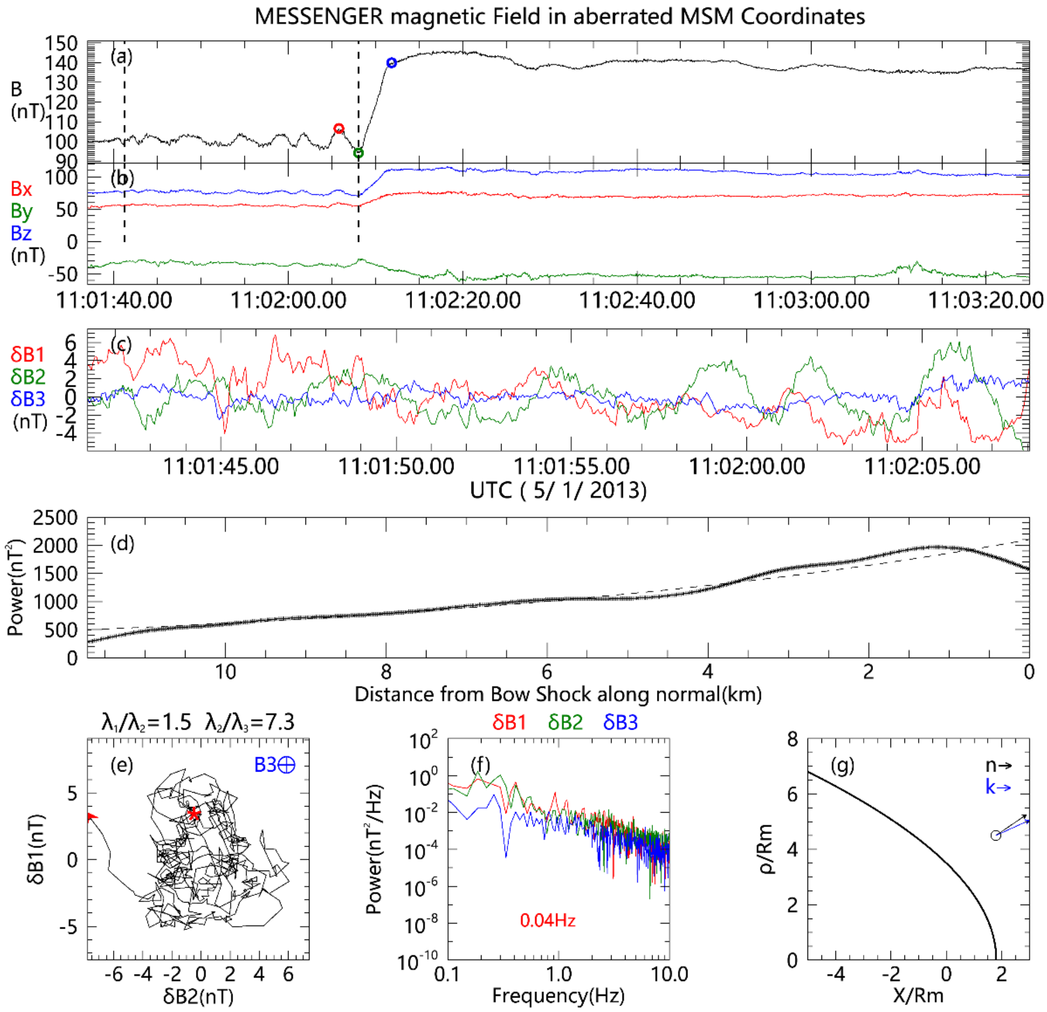
MESSENGER magnetic Field in aberrated MSM Coordinates
(a)
B (nT)
(b)
Bx
By
Bz
(nT)
11:01:40.00
11:02:00.00
11:02:20.00
11:02:40.00
11:03:00.00
11:03:20.00
(c)
δB1
δB2
δB3
(nT)
11:01:45.00
11:01:50.00
11:01:55.00
11:02:00.00
11:02:05.00
UTC (5/ 1/ 2013)
(d)
Power(nT²)
Distance from Bow Shock along normal(km)
λ₁/λ₂=1.5 λ₂/λ₃=7.3
(e)
B3⊕
δB1(nT)
δB2(nT)
δB1 δB2 δB3
(f)
Power(nT²/Hz)
0.04Hz
Frequency(Hz)
(g)
n→
k→
ρ/Rm
X/Rm

Event 22

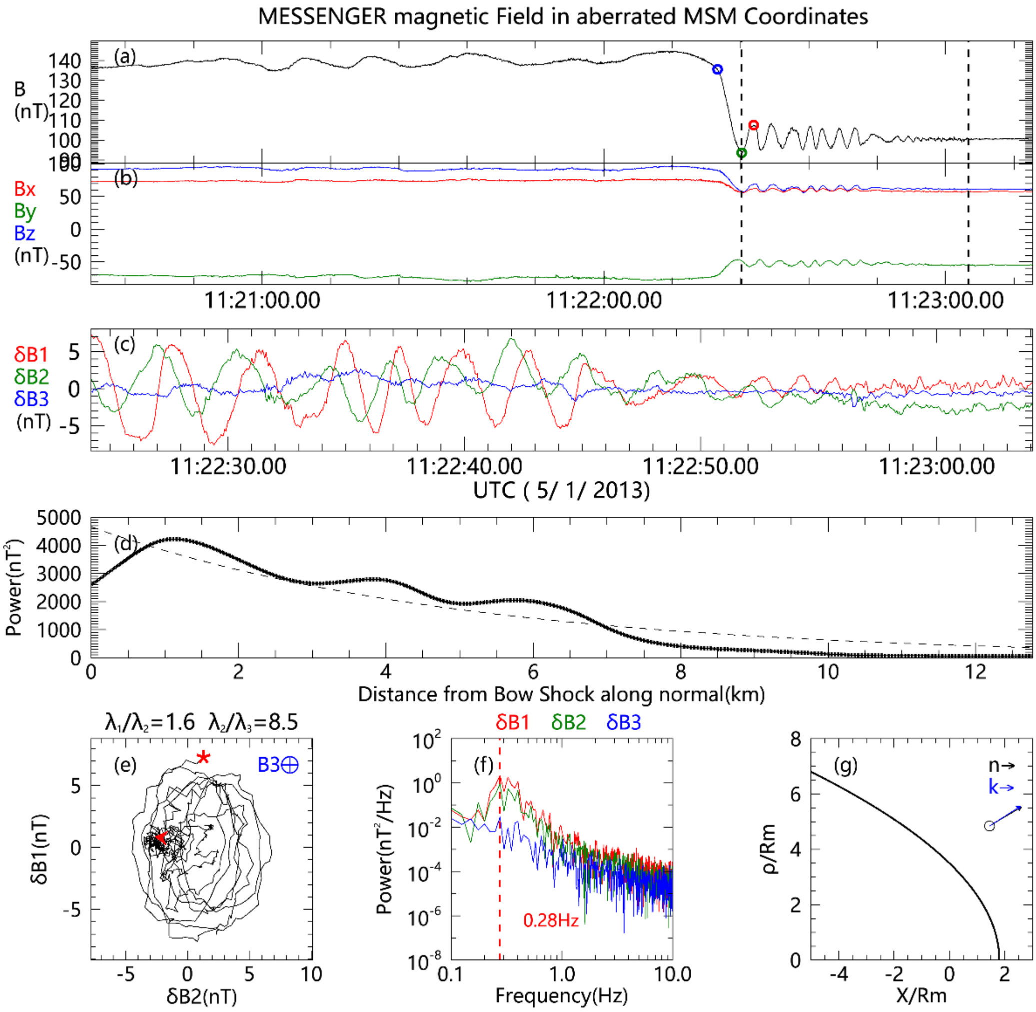
MESSENGER magnetic Field in aberrated MSM Coordinates
(a)
B (nT)
(b)
Bx
By
Bz
(nT)
11:21:00.00
11:22:00.00
11:23:00.00
(c)
δB1
δB2
δB3
(nT)
11:22:30.00
11:22:40.00
11:22:50.00
11:23:00.00
UTC (5/ 1/ 2013)
(d)
Power(nT²)
Distance from Bow Shock along normal(km)
λ₁/λ₂=1.6 λ₂/λ₃=8.5
(e)
B3⊕
δB1(nT)
δB2(nT)
δB1 δB2 δB3
(f)
0.28Hz
Power(nT²/Hz)
Frequency(Hz)
(g)
n→
k→
ρ/Rm
X/Rm

Event 23

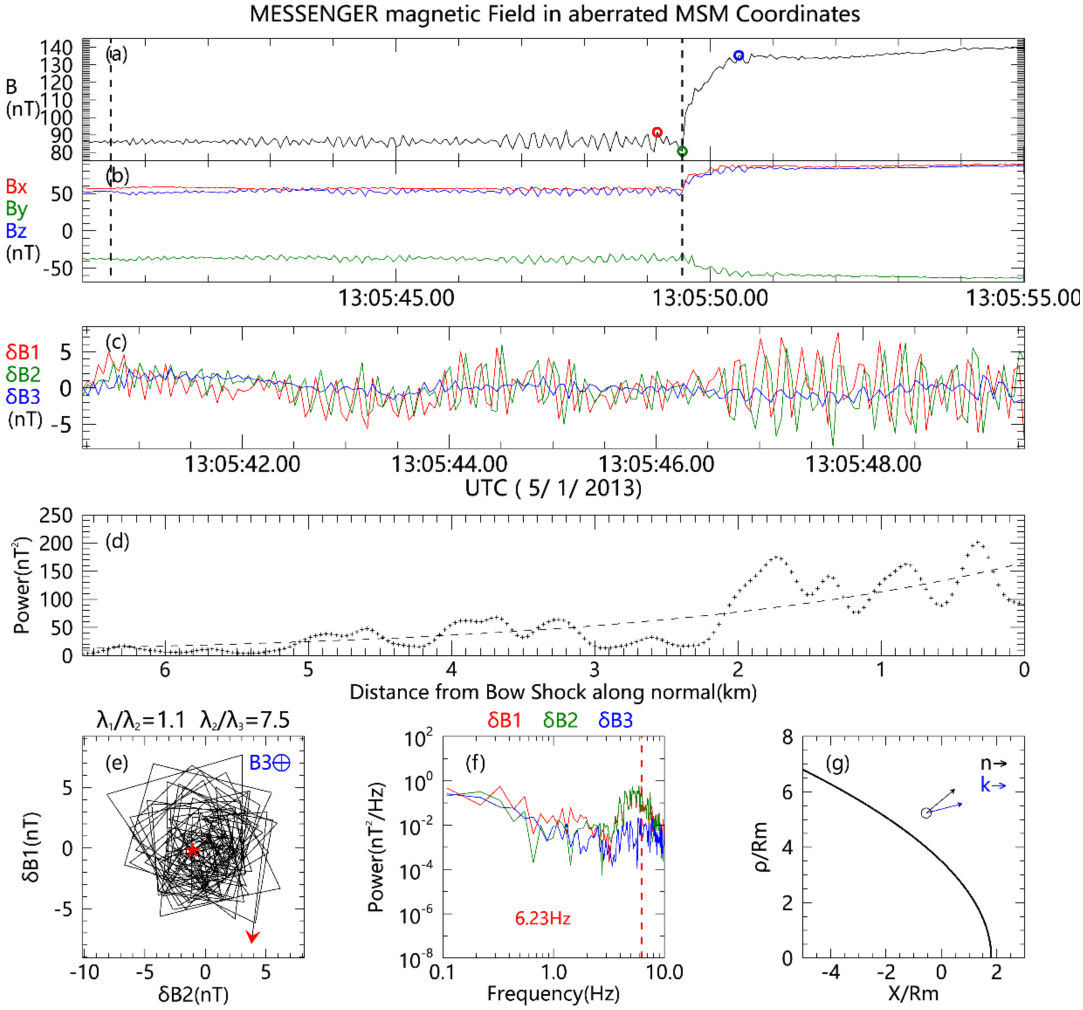

MESSENGER magnetic Field in aberrated MSM Coordinates
(a)
B (nT)
(b)
Bx
By
Bz
(nT)
13:05:45.00
13:05:50.00
13:05:55.00
(c)
δB1
δB2
δB3
(nT)
13:05:42.00
13:05:44.00
13:05:46.00
13:05:48.00
UTC (5/ 1/ 2013)
(d)
Power(nT²)
Distance from Bow Shock along normal(km)
λ₁/λ₂=1.1 λ₂/λ₃=7.5
(e)
B3⊕
δB1(nT)
δB2(nT)
(f)
δB1 δB2 δB3
Power(nT²/Hz)
6.23Hz
Frequency(Hz)
(g)
n→
k→
ρ/Rm
X/Rm

Event 24

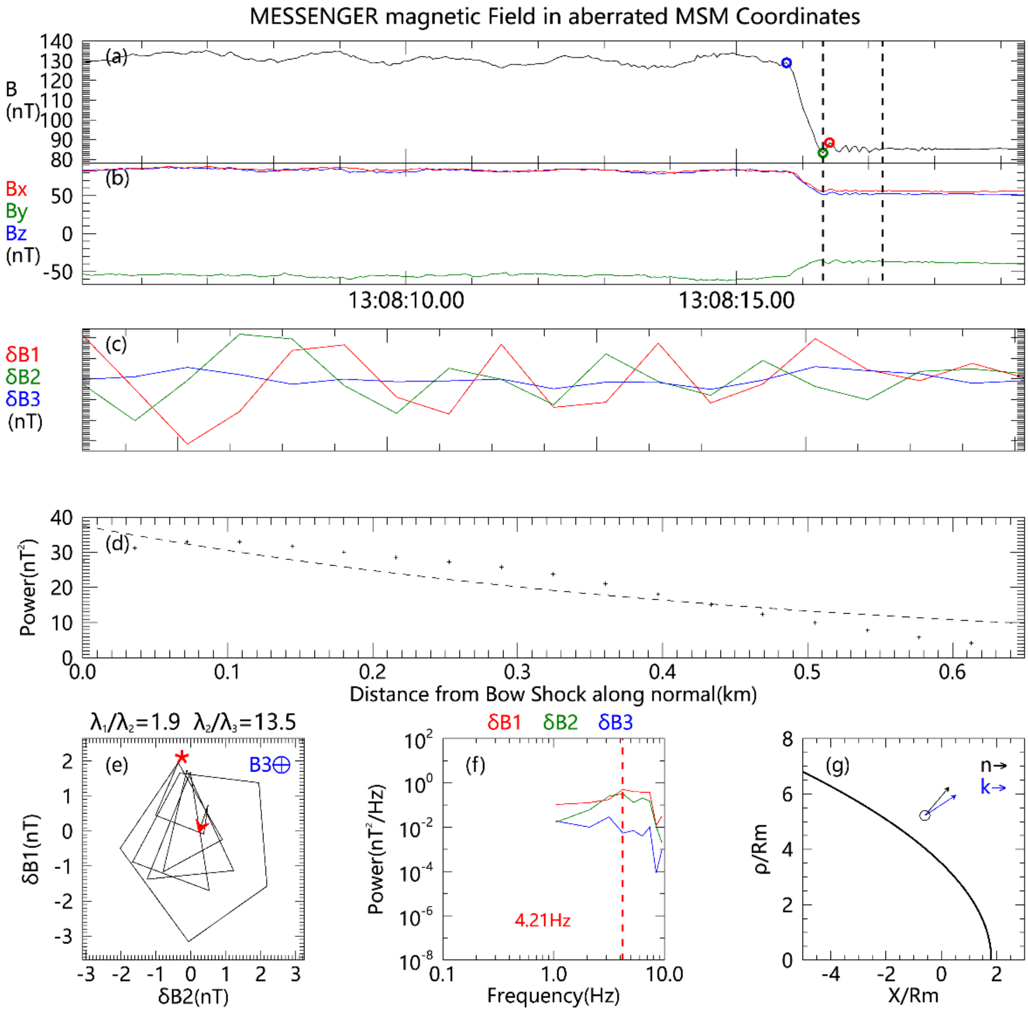

MESSENGER magnetic Field in aberrated MSM Coordinates
(a)
B (nT)
(b)
Bx
By
Bz
(nT)
13:08:10.00
13:08:15.00
(c)
δB1
δB2
δB3
(nT)
(d)
Power(nT^2)
Distance from Bow Shock along normal(km)
λ_1/λ_2=1.9 λ_2/λ_3=13.5
(e)
B3⊕
δB1(nT)
δB2(nT)
(f)
δB1 δB2 δB3
Power(nT^2/Hz)
4.21Hz
Frequency(Hz)
(g)
n→
k→
ρ/Rm
X/Rm

Event 25

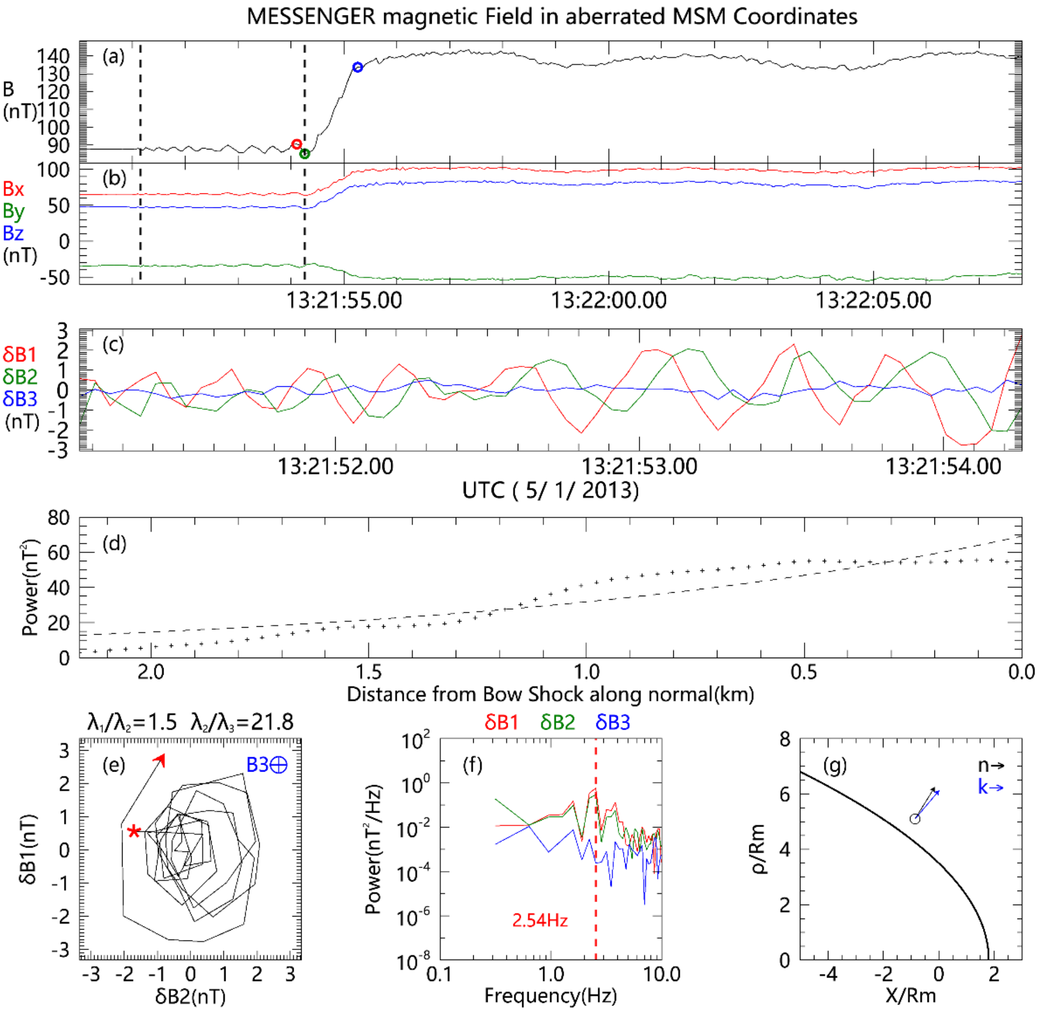

MESSENGER magnetic Field in aberrated MSM Coordinates
(a)
B (nT)
(b)
Bx
By
Bz
(nT)
13:21:55.00
13:22:00.00
13:22:05.00
(c)
δB1
δB2
δB3
(nT)
13:21:52.00
13:21:53.00
13:21:54.00
UTC (5/ 1/ 2013)
(d)
Power(nT^2)
Distance from Bow Shock along normal(km)
λ₁/λ₂=1.5 λ₂/λ₃=21.8
(e)
B3⊕
δB1(nT)
δB2(nT)
(f)
δB1 δB2 δB3
Power(nT^2/Hz)
2.54Hz
Frequency(Hz)
(g)
n→
k→
ρ/Rm
X/Rm

Event 26

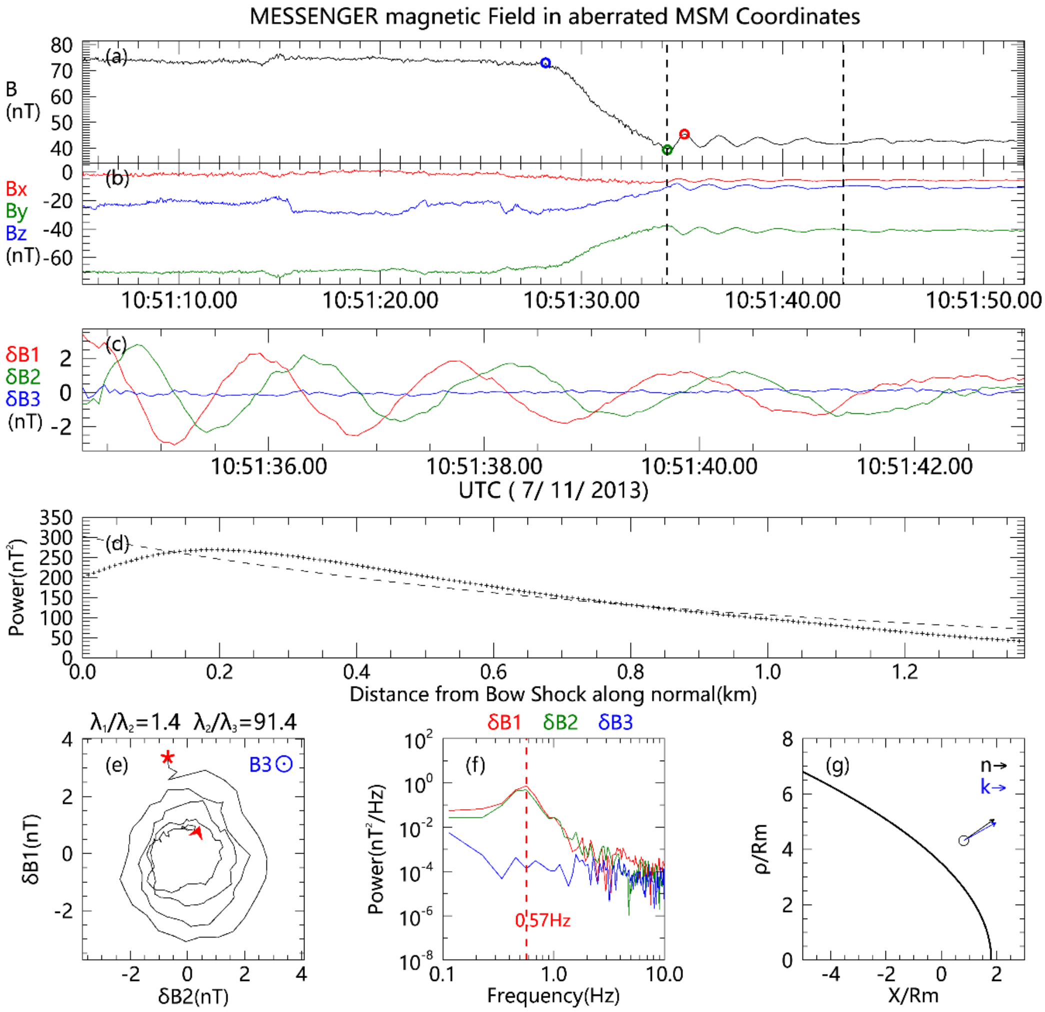

MESSENGER magnetic Field in aberrated MSM Coordinates
(a)
B (nT)
(b)
Bx
By
Bz
(nT)
10:51:10.00
10:51:20.00
10:51:30.00
10:51:40.00
10:51:50.00
(c)
δB1
δB2
δB3
(nT)
10:51:36.00
10:51:38.00
10:51:40.00
10:51:42.00
UTC (7/ 11/ 2013)
(d)
Power(nT²)
Distance from Bow Shock along normal(km)
λ1/λ2=1.4 λ2/λ3=91.4
(e)
B3
δB1(nT)
δB2(nT)
(f)
δB1 δB2 δB3
Power(nT²/Hz)
0.57Hz
Frequency(Hz)
(g)
n→
k→
ρ/Rm
X/Rm

Event 27

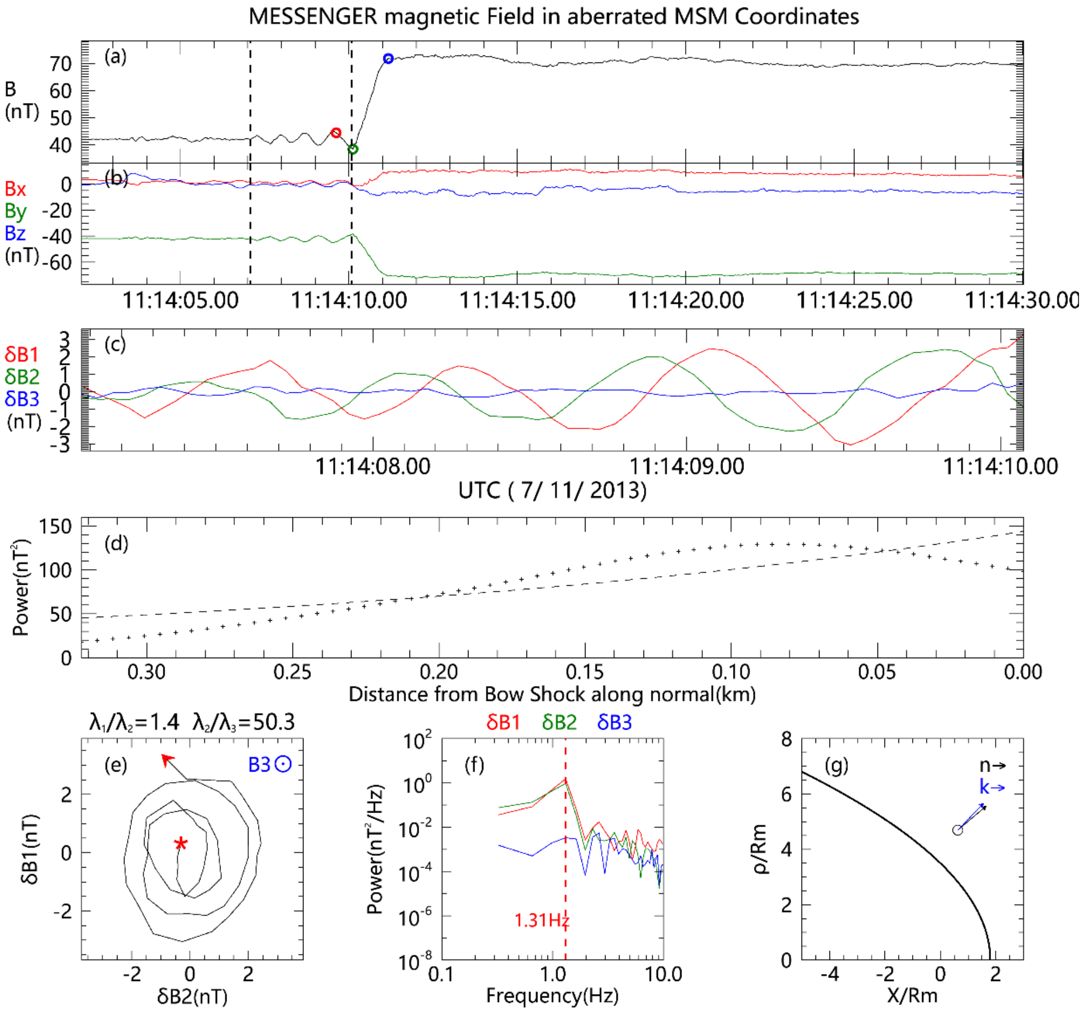

MESSENGER magnetic Field in aberrated MSM Coordinates
(a)
B (nT)
70
60
50
40
(b)
Bx
By
Bz
(nT)
0
-20
-40
-60
11:14:05.00
11:14:10.00
11:14:15.00
11:14:20.00
11:14:25.00
11:14:30.00
(c)
δB1
δB2
δB3
(nT)
11:14:08.00
11:14:09.00
11:14:10.00
UTC (7/ 11/ 2013)
(d)
Power(nT²)
150
100
50
0
0.30
0.25
0.20
0.15
0.10
0.05
0.00
Distance from Bow Shock along normal(km)
λ1/λ2=1.4 λ2/λ3=50.3
(e)
B3
δB1(nT)
δB2(nT)
(f)
δB1 δB2 δB3
Power(nT²/Hz)
1.31Hz
Frequency(Hz)
0.1
1.0
10.0
(g)
n→
k→
ρ/Rm
X/Rm

Event 28

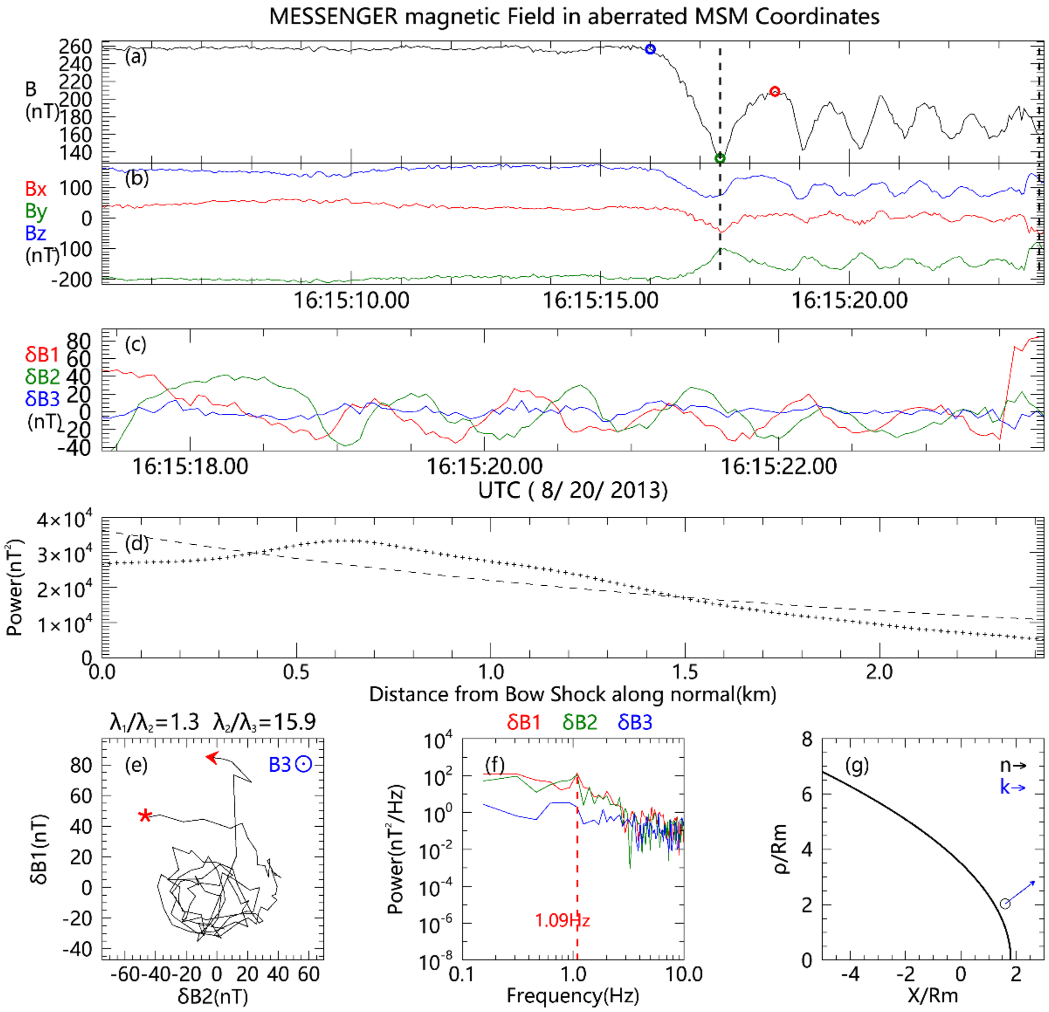

MESSENGER magnetic Field in aberrated MSM Coordinates
(a)
B (nT)
(b)
Bx By Bz (nT)
16:15:10.00
16:15:15.00
16:15:20.00
(c)
δB1 δB2 δB3 (nT)
16:15:18.00
16:15:20.00
16:15:22.00
UTC (8/ 20/ 2013)
(d)
Power(nT^2)
Distance from Bow Shock along normal(km)
λ_1/λ_2=1.3 λ_2/λ_3=15.9
(e)
B3
δB1(nT)
δB2(nT)
δB1 δB2 δB3
(f)
Power(nT^2/Hz)
1.09Hz
Frequency(Hz)
(g)
n→
k→
ρ/Rm
X/Rm

Event 29

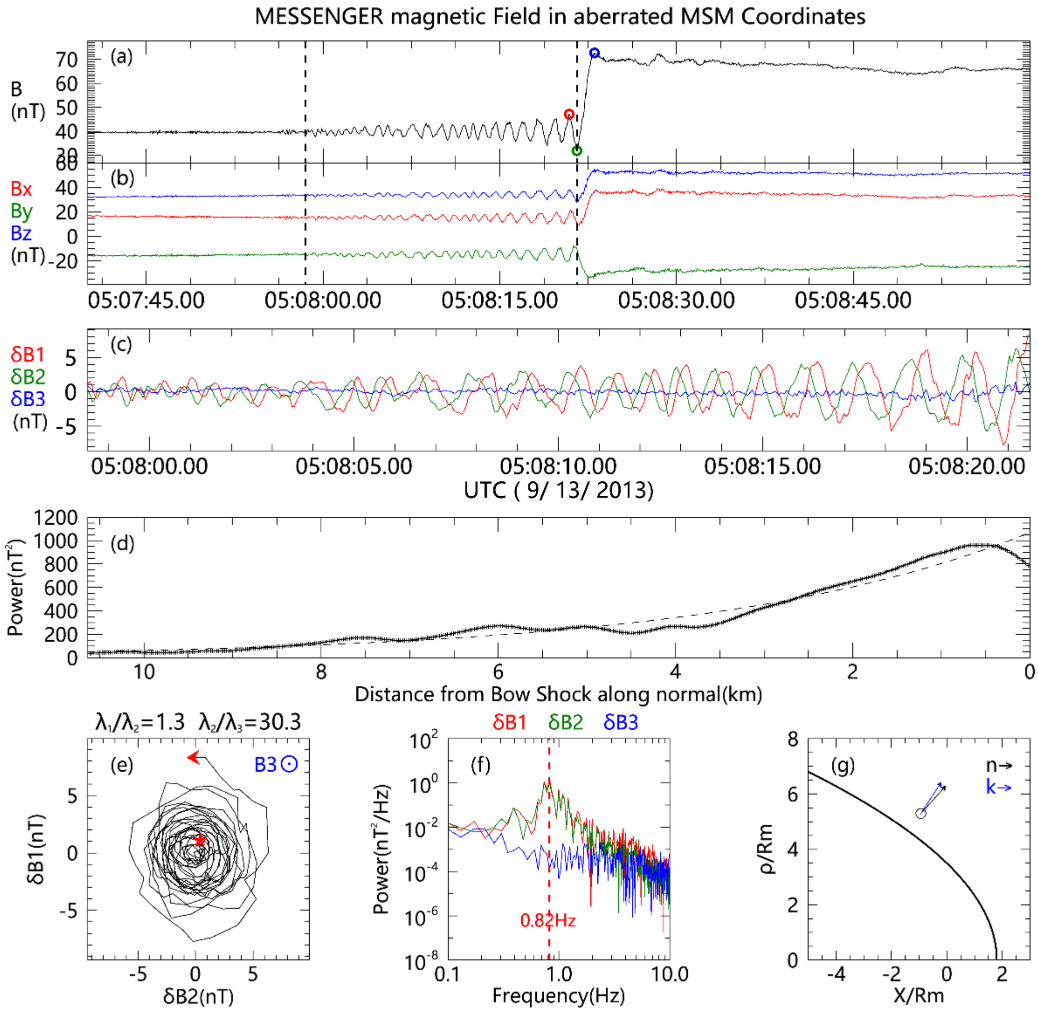

MESSENGER magnetic Field in aberrated MSM Coordinates
(a)
B (nT)
(b)
Bx
By
Bz
(nT)
05:07:45.00
05:08:00.00
05:08:15.00
05:08:30.00
05:08:45.00
(c)
δB1
δB2
δB3
(nT)
05:08:00.00
05:08:05.00
05:08:10.00
05:08:15.00
05:08:20.00
UTC (9/ 13/ 2013)
(d)
Power(nT^2)
Distance from Bow Shock along normal(km)
λ_1/λ_2=1.3 λ_2/λ_3=30.3
(e)
B3
δB1(nT)
δB2(nT)
(f)
δB1 δB2 δB3
Power(nT^2/Hz)
0.82Hz
Frequency(Hz)
(g)
n
k
ρ/Rm
X/Rm

Event 30

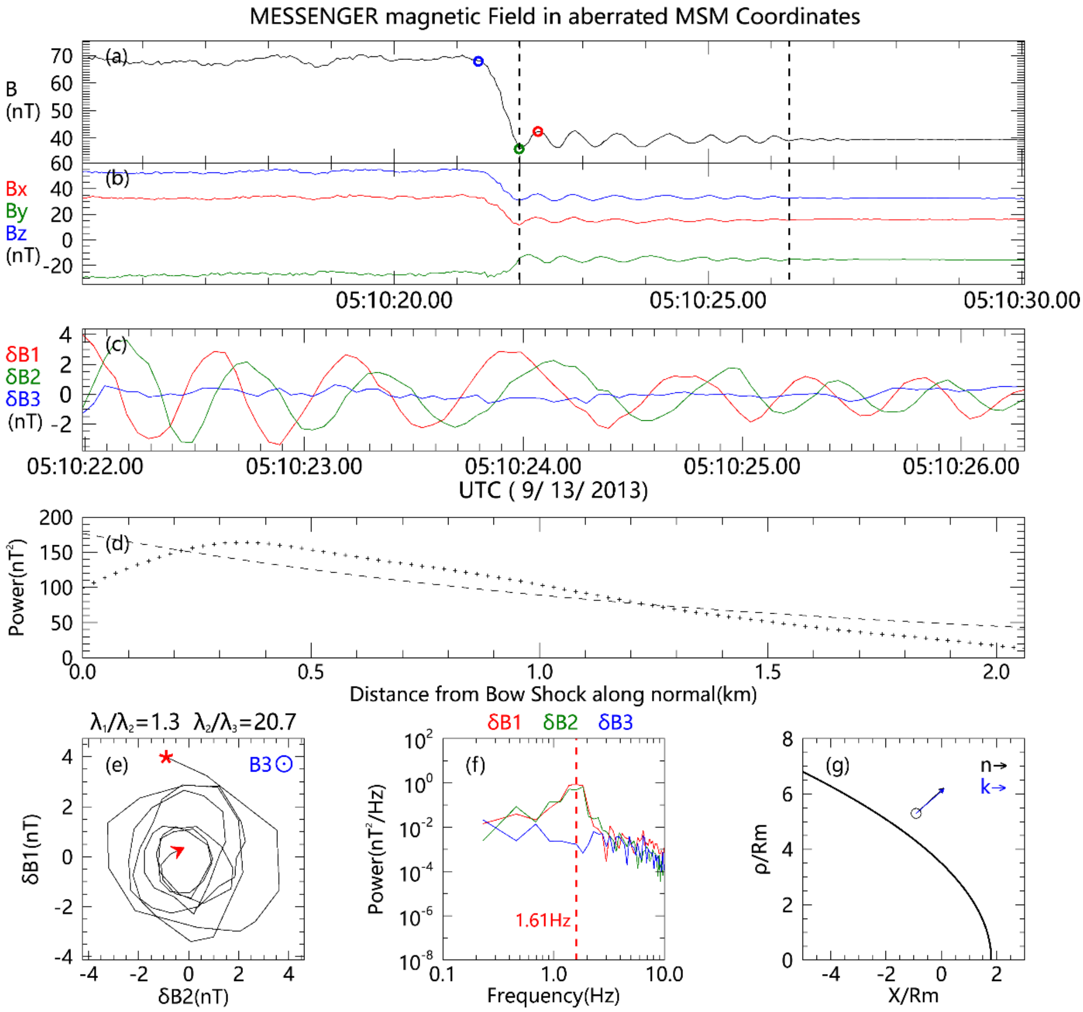

MESSENGER magnetic Field in aberrated MSM Coordinates
(a)
B (nT)
(b)
Bx
By
Bz
(nT)
05:10:20.00
05:10:25.00
05:10:30.00
(c)
δB1
δB2
δB3
(nT)
05:10:22.00
05:10:23.00
05:10:24.00
05:10:25.00
05:10:26.00
UTC (9/ 13/ 2013)
(d)
Power(nT^2)
Distance from Bow Shock along normal(km)
λ_1/λ_2=1.3 λ_2/λ_3=20.7
(e)
B3
δB1(nT)
δB2(nT)
δB1 δB2 δB3
(f)
Power(nT^2/Hz)
1.61Hz
Frequency(Hz)
(g)
n→
k→
ρ/Rm
X/Rm

Event 31

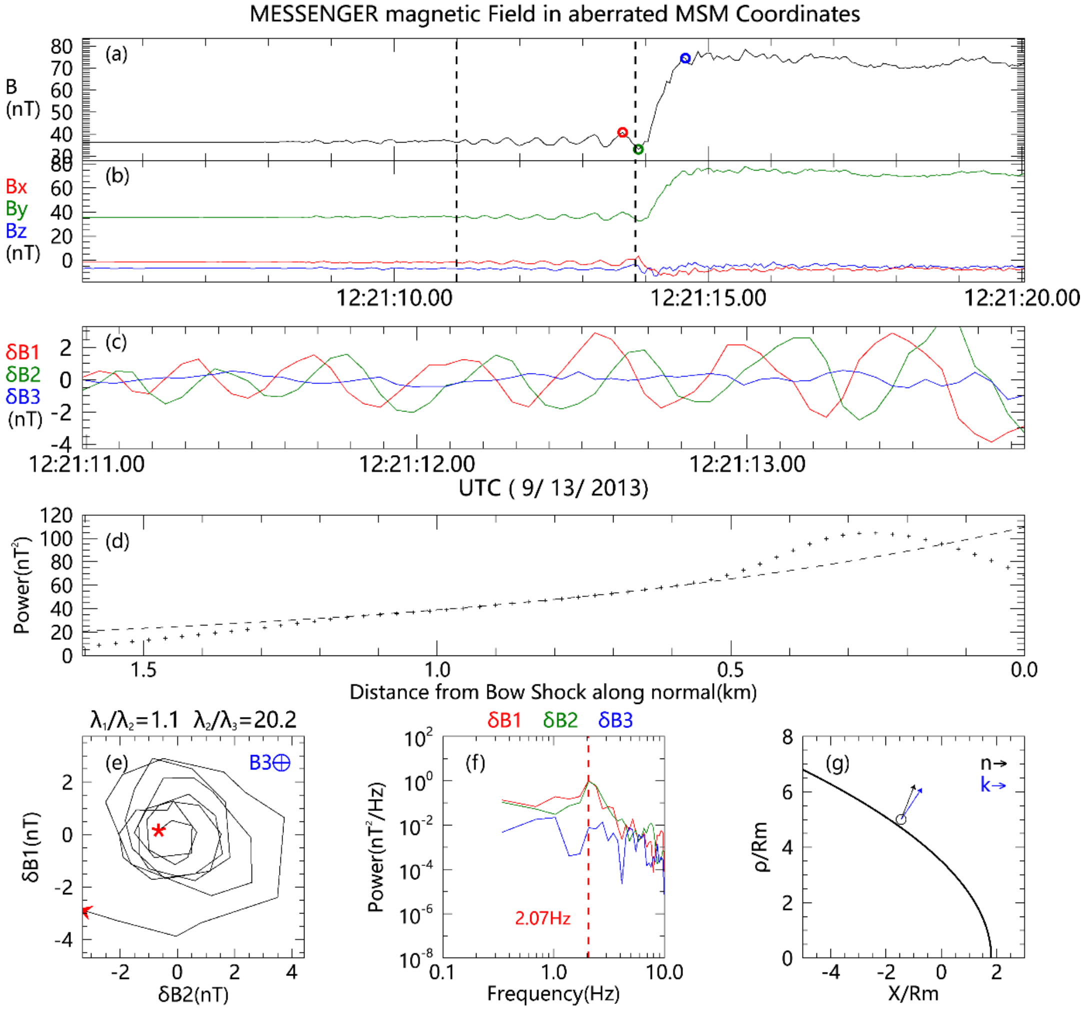

MESSENGER magnetic Field in aberrated MSM Coordinates
(a)
B (nT)
(b)
Bx
By
Bz
(nT)
12:21:10.00
12:21:15.00
12:21:20.00
(c)
δB1
δB2
δB3
(nT)
12:21:11.00
12:21:12.00
12:21:13.00
UTC (9/ 13/ 2013)
(d)
Power(nT^2)
Distance from Bow Shock along normal(km)
λ_1/λ_2=1.1 λ_2/λ_3=20.2
(e)
B3⊕
δB1(nT)
δB2(nT)
(f)
δB1 δB2 δB3
Power(nT^2/Hz)
2.07Hz
Frequency(Hz)
(g)
n→
k→
ρ/Rm
X/Rm

Event 32

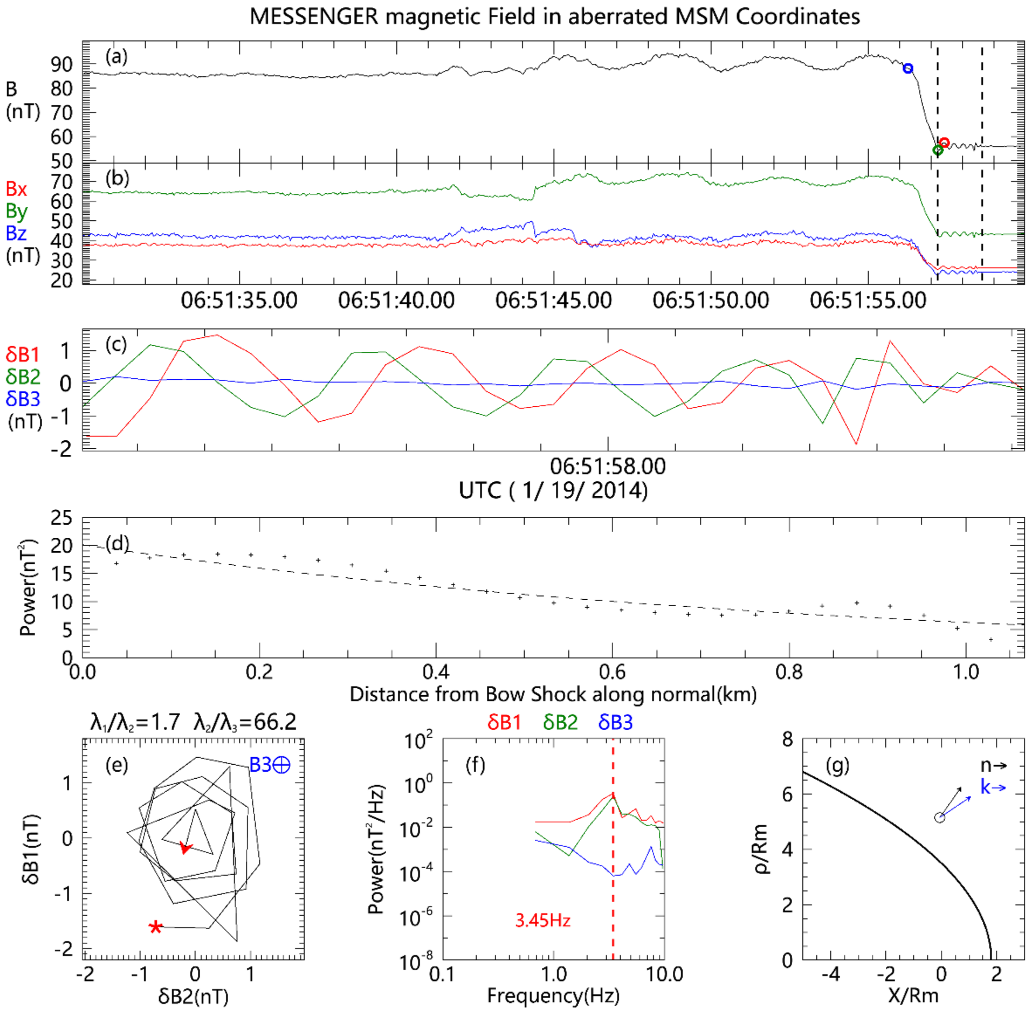
MESSENGER magnetic Field in aberrated MSM Coordinates
(a)
B (nT)
(b)
Bx
By
Bz
(nT)
06:51:35.00
06:51:40.00
06:51:45.00
06:51:50.00
06:51:55.00
(c)
δB1
δB2
δB3
(nT)
06:51:58.00
UTC (1/ 19/ 2014)
(d)
Power(nT²)
Distance from Bow Shock along normal(km)
λ1/λ2=1.7 λ2/λ3=66.2
(e)
B3⊕
δB1(nT)
δB2(nT)
δB1 δB2 δB3
(f)
Power(nT²/Hz)
3.45Hz
Frequency(Hz)
(g)
n→
k→
ρ/Rm
X/Rm

Event 33

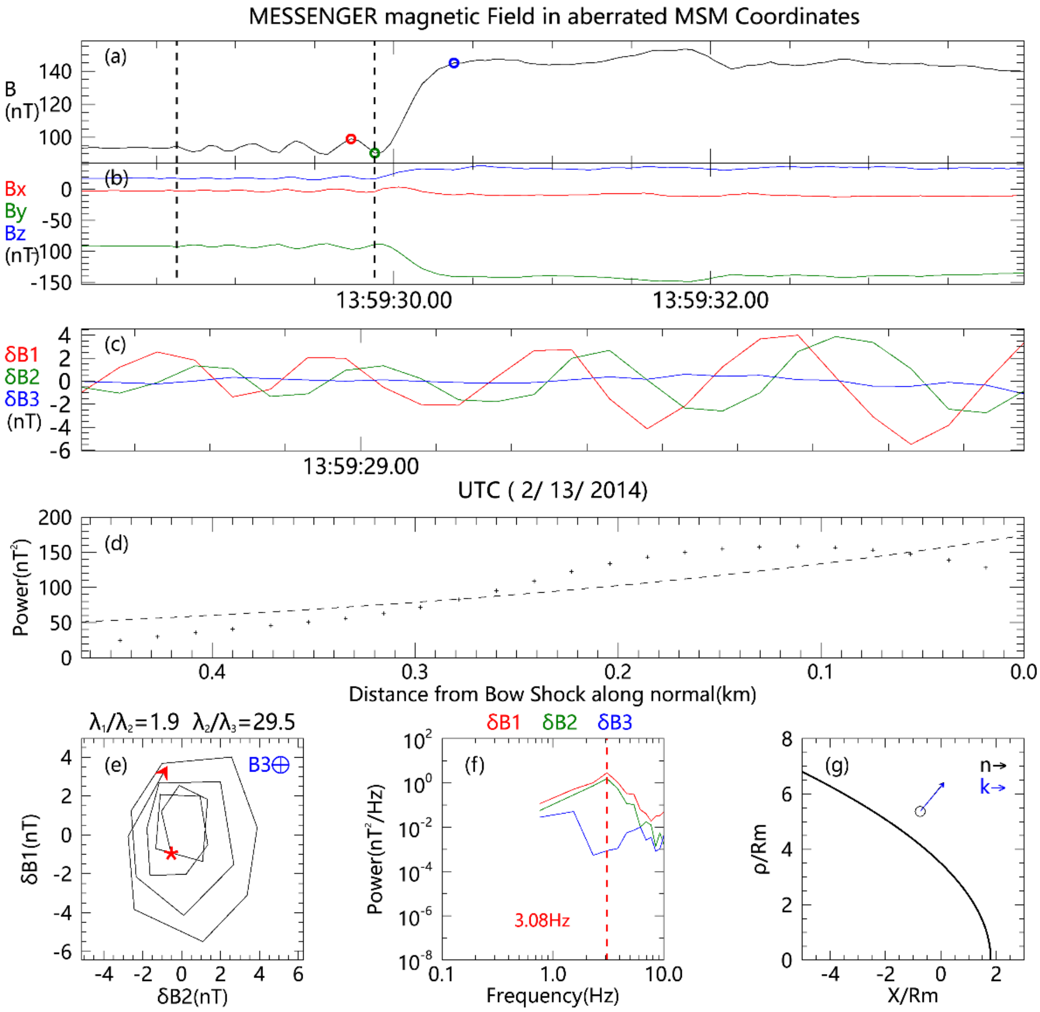

MESSENGER magnetic Field in aberrated MSM Coordinates
(a)
B
(nT)
140
120
100
(b)
Bx
By
Bz
(nT)
0
-50
-100
-150
13:59:30.00
13:59:32.00
(c)
δB1
δB2
δB3
(nT)
13:59:29.00
UTC (2/ 13/ 2014)
(d)
Power(nT²)
Distance from Bow Shock along normal(km)
λ₁/λ₂=1.9 λ₂/λ₃=29.5
(e)
B3⊕
δB1(nT)
δB2(nT)
(f)
δB1 δB2 δB3
Power(nT²/Hz)
3.08Hz
Frequency(Hz)
(g)
n→
k→
ρ/Rm
X/Rm

Event 34

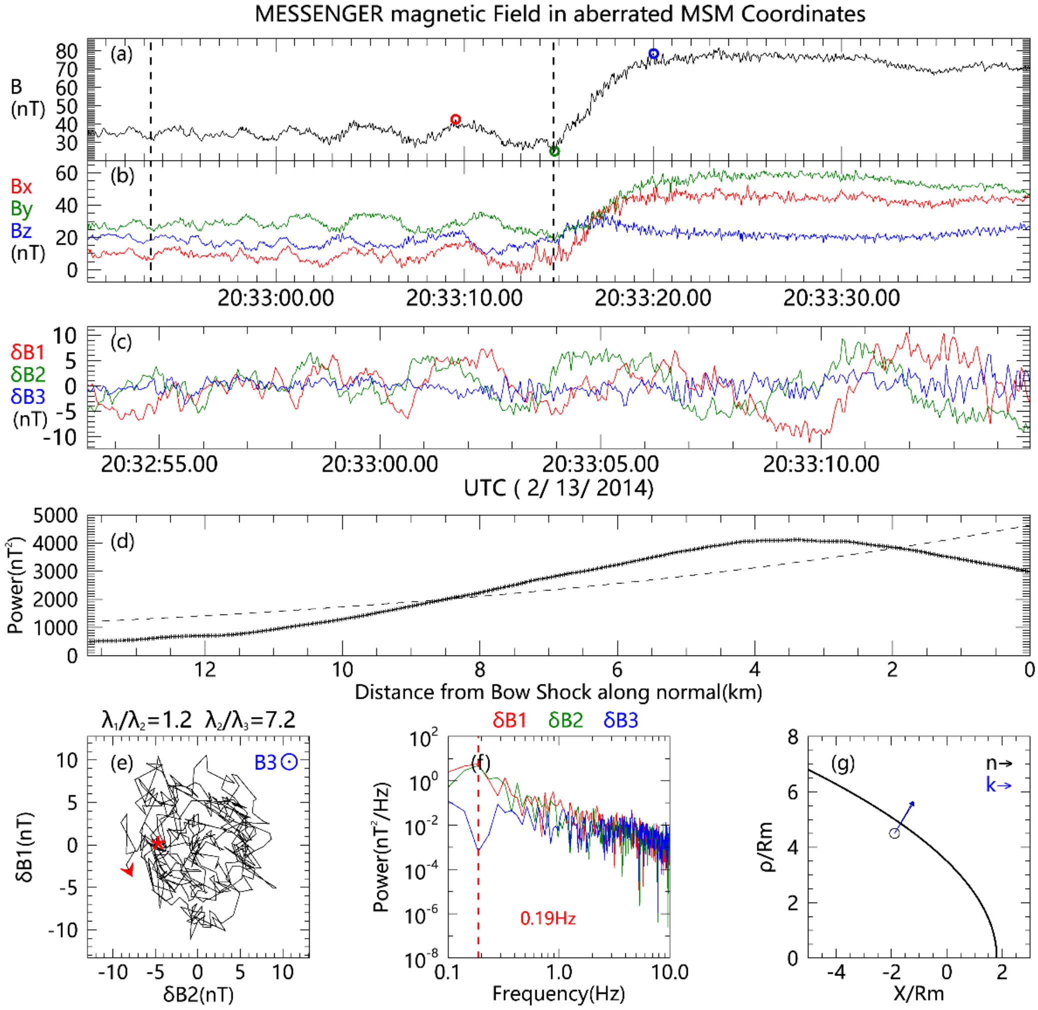

MESSENGER magnetic Field in aberrated MSM Coordinates
(a)
B (nT)
(b)
Bx
By
Bz
(nT)
20:33:00.00
20:33:10.00
20:33:20.00
20:33:30.00
(c)
δB1
δB2
δB3
(nT)
20:32:55.00
20:33:00.00
20:33:05.00
20:33:10.00
UTC (2/ 13/ 2014)
(d)
Power(nT^2)
Distance from Bow Shock along normal(km)
λ1/λ2=1.2 λ2/λ3=7.2
(e)
B3
δB1(nT)
δB2(nT)
δB1 δB2 δB3
(f)
Power(nT^2/Hz)
0.19Hz
Frequency(Hz)
(g)
n
k
ρ/Rm
X/Rm

Event 35

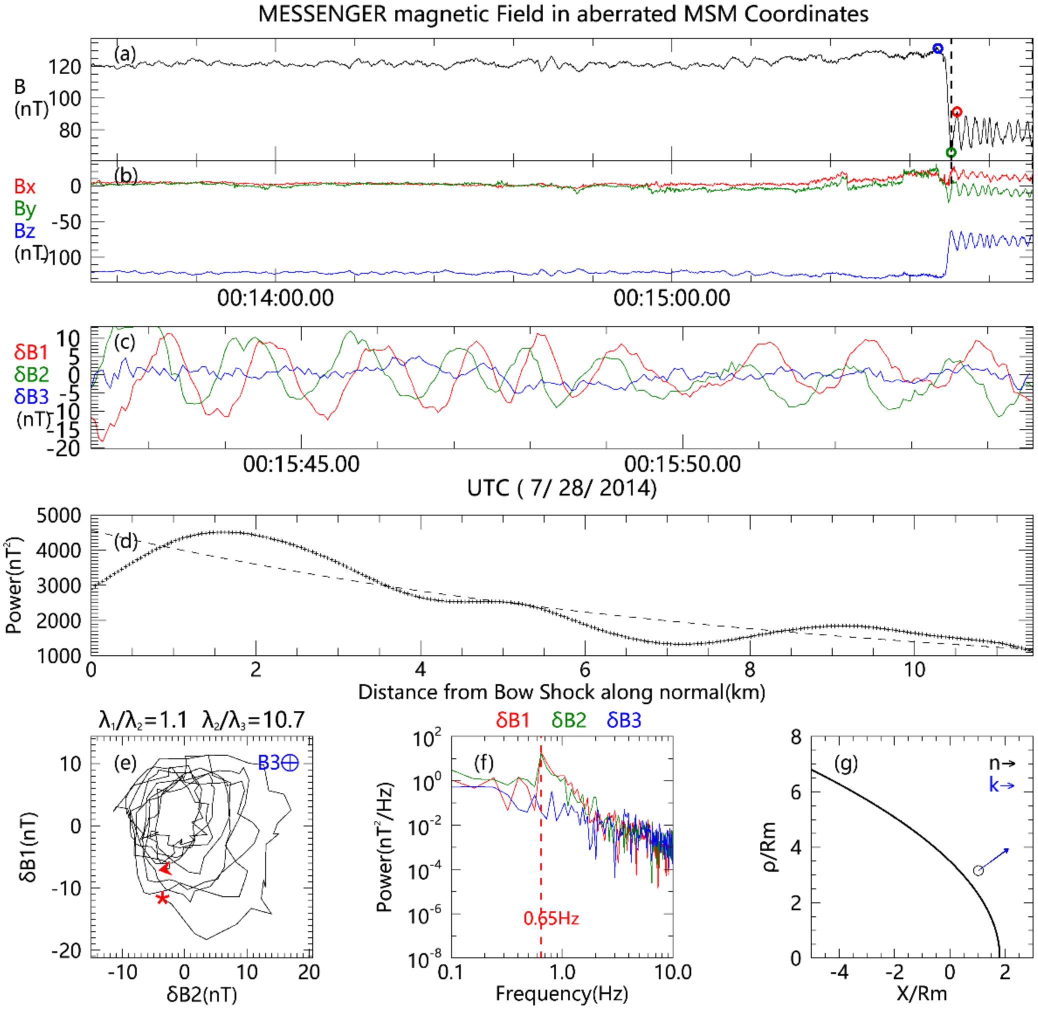

MESSENGER magnetic Field in aberrated MSM Coordinates
(a)
B (nT)
120
100
80
(b)
Bx
By
Bz
(nT)
0
-50
-100
00:14:00.00
00:15:00.00
(c)
δB1
δB2
δB3
(nT)
10
5
0
-5
-10
-15
-20
00:15:45.00
00:15:50.00
UTC (7/ 28/ 2014)
(d)
Power(nT^2)
5000
4000
3000
2000
1000
0
2
4
6
8
10
Distance from Bow Shock along normal(km)
λ1/λ2=1.1 λ2/λ3=10.7
(e)
B3⊕
δB1(nT)
δB2(nT)
10
0
-10
-20
20
δB1 δB2 δB3
(f)
Power(nT^2/Hz)
10^2
10^0
10^-2
10^-4
10^-6
10^-8
0.1
1.0
10.0
0.65Hz
Frequency(Hz)
(g)
n→
k→
ρ/Rm
X/Rm
8
6
4
2
0
-4
-2
0
2

Event 36

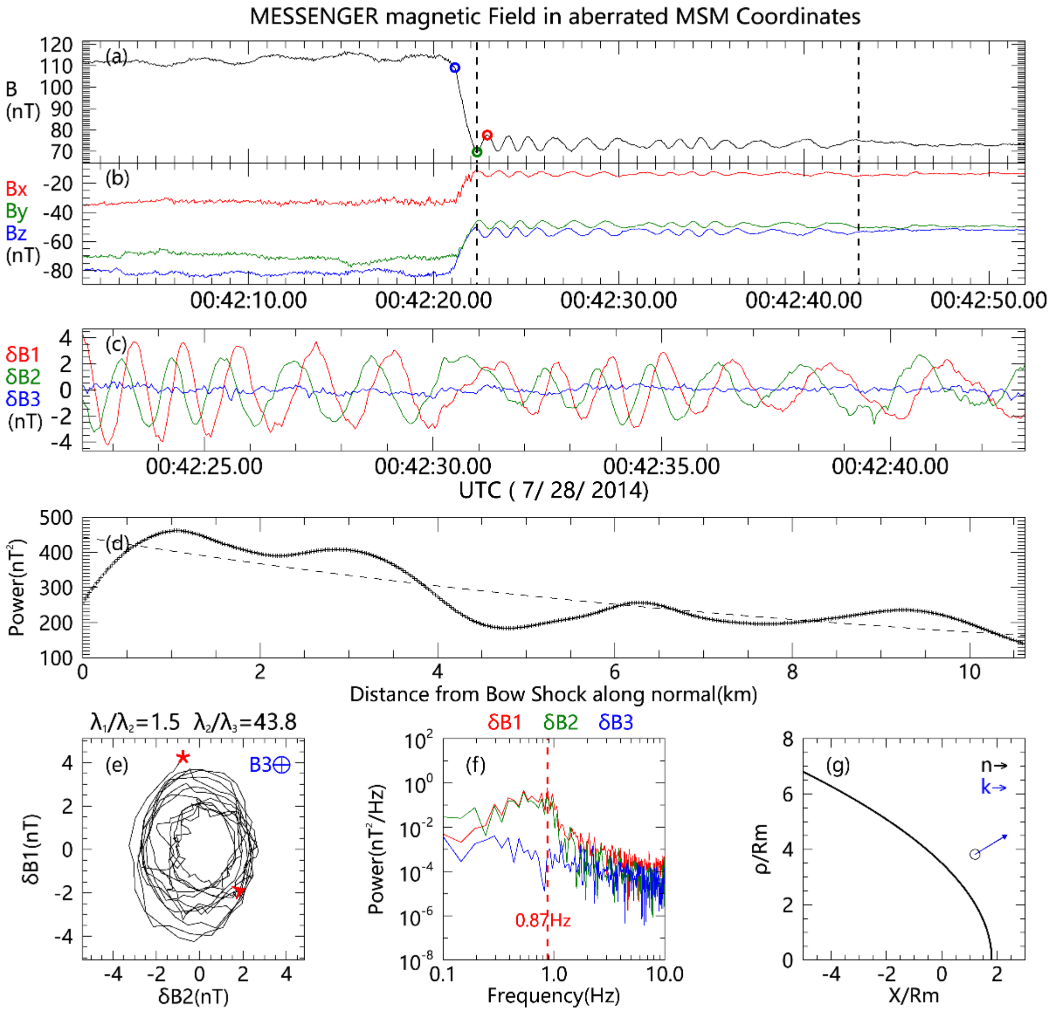

MESSENGER magnetic Field in aberrated MSM Coordinates
(a)
B (nT)
(b)
Bx
By
Bz
(nT)
00:42:10.00
00:42:20.00
00:42:30.00
00:42:40.00
00:42:50.00
(c)
δB1
δB2
δB3
(nT)
00:42:25.00
00:42:30.00
00:42:35.00
00:42:40.00
UTC (7/ 28/ 2014)
(d)
Power(nT²)
Distance from Bow Shock along normal(km)
λ₁/λ₂=1.5 λ₂/λ₃=43.8
(e)
B3⊕
δB1(nT)
δB2(nT)
δB1 δB2 δB3
(f)
Power(nT²/Hz)
0.87Hz
Frequency(Hz)
(g)
n→
k→
ρ/Rm
X/Rm